

Benchmarking the Robustness of Image Watermarks

Bang An^{*1}, Mucong Ding^{*1}, Tahseen Rabbani^{*1}, Aakriti Agrawal¹, Yuancheng Xu¹, Chenghao Deng¹,
Sicheng Zhu¹, Abdirisak Mohamed^{1,2}, Yuxin Wen¹, Tom Goldstein¹, Furong Huang¹

¹University of Maryland, ²SAP Labs, LLC.

{bangan, mcding, trabbani, agrawal5, ycxu, dengch16, sczhu, amoham70, ywen, tomg, furongh}@umd.edu

Abstract

This paper investigates the weaknesses of image watermarking techniques. We present WAVES (Watermark Analysis via Enhanced Stress-testing), a novel benchmark for assessing watermark robustness, overcoming the limitations of current evaluation methods. WAVES integrates detection and identification tasks and establishes a standardized evaluation protocol comprised of a diverse range of stress tests. The attacks in WAVES range from traditional image distortions to advanced and novel variations of diffusive, and adversarial attacks. Our evaluation examines two pivotal dimensions: the degree of image quality degradation and the efficacy of watermark detection after attacks. We develop a series of Performance vs. Quality 2D plots, varying over several prominent image similarity metrics, which are then aggregated in a heuristically novel manner to paint an overall picture of watermark robustness and attack potency. Our comprehensive evaluation reveals previously undetected vulnerabilities of several modern watermarking algorithms. We envision WAVES as a toolkit for the future development of robust watermarking systems. The project is available at <https://wavesbench.github.io/>.

1 Introduction

Recent and pivotal advancements in text-to-image diffusion models (Dhariwal and Nichol, 2021, Ho et al., 2020, Rombach et al., 2022) have garnered the attention of the AI community and the general public. Open-source models such as Stable Diffusion and proprietary models such as the Dall-E family and Midjourney have enabled users to produce images that are of human-produced quality. Consequently, there has been a strong push in AI/ML community to develop reliable algorithms for detecting AI-generated content and determining its source (Executive Office of the President, 2023).

One avenue for maintaining the provenance of generative content is by embedding *watermarks*. A watermark is a signal encoded onto an image to signify its source or ownership (Al-Haj, 2007, Fernandez et al., 2023, Tancik et al., 2020, Wen et al., 2023, Zhang et al., 2019, Zhu et al., 2018). To avoid degradation of image quality, an invisible watermark is desired. Many such watermarks are robust to common image manipulations (Fernandez et al., 2023, Lukas et al., 2023, Wen et al., 2023, Zhao et al., 2023a), and adversarial efforts to remove the watermark are complicated by the difficulty of decoding/extracting the message without private knowledge of the watermarking scheme (Fernandez et al., 2023, Tancik et al., 2020). Despite this difficulty, various watermark removal schemes can still be effective (Saber et al., 2023, Zhao et al., 2023a). However, a lack of standardized evaluations in existing literature (i.e., inconsistent image quality measures, statistical parameters, and types of attacks) has resulted in an incomplete picture of the vulnerabilities and robustness of these algorithms in the real world.

In this work, we present WAVES (Watermark Analysis via Enhanced Stress-testing), a novel benchmark for assessing watermark robustness, overcoming the limitations of current evaluation methods.

*Co-first-authors with equal contribution. First authors are ordered alphabetically.

Our benchmark consists of a comprehensive variety of novel and realistic attacks, including classical image distortions, image regeneration (Zhao et al., 2023a), and adversarial attacks. In an effort to stress-test existing and future watermarks, we propose several new attacks such as adversarial embedding attacks, and new variants of existing attacks such as multi-regeneration attacks.

WAVES focuses on the sensitivity and robustness of watermark detection, measured by the true positive rate (TPR) at 0.1% false positive rate (FPR), and studies the severity of image degradations needed to decrease this sensitivity. We declare a watermark detected if it is present with a threshold level of statistical significance ($\alpha = 0.001$), and measure the severity of image degradation with multiple quality metrics including PSNR (Hore and Ziou, 2010), LPIPS (Zhang et al., 2018), CLIP-FID (Kynkäänniemi et al., 2019), and more. We conduct thorough evaluations with images from DiffusionDB (Wang et al., 2022), MS-COCO (Lin et al., 2014), and the DALL-E3 datasets.

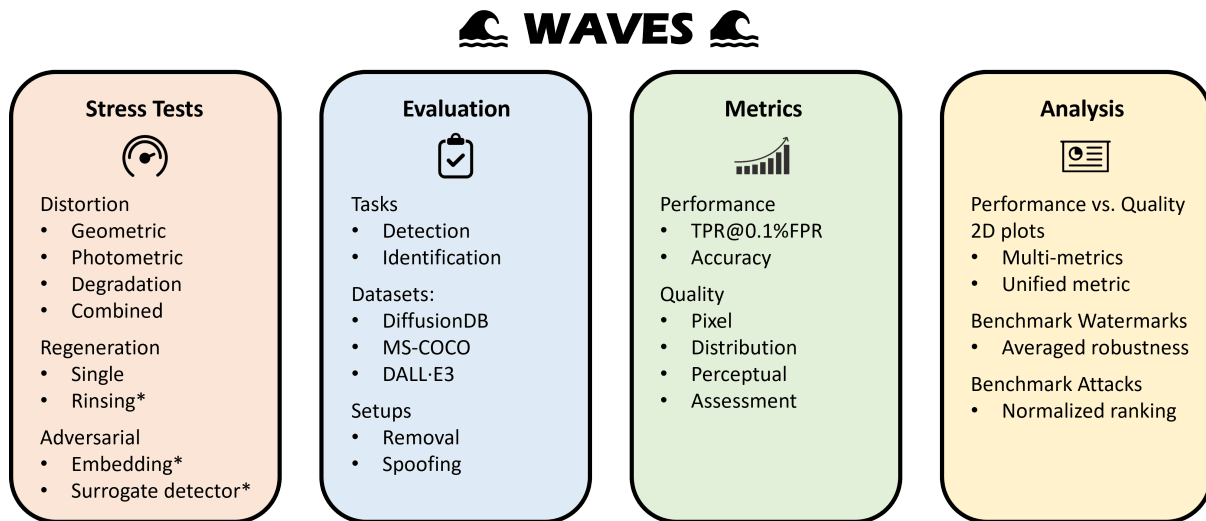


Figure 1. **WAVES (Watermark Analysis via Enhanced Stress-testing)**: a comprehensive benchmark for assessing watermark robustness. WAVES includes a diverse range of stress tests and establishes unified evaluation metrics. WAVES incorporates most existing watermark attacks and proposes new, stronger attacks (marked with * in this figure) in the stress tests, establishing new testing standards for image watermark robustness.

We extensively evaluate the security of three prominent watermarking algorithms, Stable Signature (Fernandez et al., 2023), Tree-Ring (Wen et al., 2023), and StegStamp (Tancik et al., 2020), respectively representing three major techniques for embedding an invisible signature: in-processing via model modification, in-processing via random seed modification, and post-processing (detailed in Section 2.1).

The WAVES framework effectively reveals weaknesses in widely used watermarking methods against both simple and sophisticated ML-based attacks. For example, watermarking algorithms using publicly available VAEs can have their watermarks effectively removed with minimal image manipulation. DALL-E3’s usage of an open-source KL-VAE underscores the need for unique VAEs in such systems.

In this paper, Section 2 provides a comprehensive summary of popular watermarking methods and existing attacks. Section 3 introduces WAVES, detailing our standardized evaluation workflow, metrics, and a range of attacks used for stress-testing. Finally, Section 4 presents our benchmarking results, in-depth analyses, and key takeaway messages.

Our contributions are summarized as follows:

1. In practical scenarios where false alarms incur high costs, our evaluation metric for watermark detection prioritizes the True Positive Rate (TPR) at a stringent False Positive Rate (FPR) threshold, specifically

0.1%. This focus addresses the inadequacies of alternative metrics such as the p -value and Area Under the Receiver Operating Characteristic (AUROC). The reliance of the p -value on distribution assumptions often leads to misleading interpretations in the face of non-standard or intricate distributions commonly seen in real-world datasets. Moreover, a high AUROC score may not necessarily imply an equally high TPR at low FPR levels — a critical consideration in watermark detection, where overlooking a genuine watermark (low TPR) at rigorous FPR thresholds can have substantial consequences.

2. Additionally, our metric incorporates image quality alongside TPR at the 0.1% FPR threshold. This integration acknowledges the necessity of maintaining a balance between the accuracy of watermark detection and the practical utility of the image. It ensures that the application of watermark detection algorithms does not compromise image quality excessively. Such a dual focus is vital in applications where maintaining both the integrity of the image and the efficacy of watermark detection is crucial.
3. We introduce a comprehensive taxonomy of attacks that encompasses classical distortions (blurring, rotation, cropping, etc.) and novel variations of regeneration and adversarial attacks, against watermarks. Our attack list is of wide breadth and includes several powerful, yet realistic manipulations. We contribute several novel attacks, such as rinsing regenerations which leverage multiple consecutive regenerations, and adversarial embedding attacks which disrupt latent features.
4. We standardize the evaluation of watermark robustness. We formalize the watermark *detection* and user *identification* problems and evaluate the robustness under both scenarios. Our evaluation jointly considers watermark decodability and image quality after attacks and integrates multiple quality metrics into a comprehensive one. Our framework benchmarks both watermark robustness and attack potency.
5. Our benchmark uncovers several especially harmful attacks for popular watermarks, some of which are first introduced in this work, underscoring the need for refinement of existing watermarking algorithms and the systems that deploy them.

2 Image Watermarks

Figure 2 depicts our scenario of interest. First, an AI company/owner embeds a watermark into its generated images. Then, if the owner is shown one of their watermarked images at a later point in time, they can identify ownership of it by recovering the watermark message. Commonly, users might modify watermarked images for legitimate personal purposes. There are also instances where users attempt to erase a watermark for malicious reasons, such as disseminating fake information or infringing upon copyright. For simplicity, we term any image manipulation as an “attack.” This paper focuses on evaluating the robustness of watermarking methods, ensuring that the image owner can still discern the watermark message even after attacks. This section reviews and categorizes current watermarking methods.

2.1 Watermarking AI-generated Images

Imprinting invisible watermarks into digital images has a long and rich history. From conventional steganography to recent generative model-based methods, we review existing watermarking methods and general approaches to watermark removal. We precisely define a taxonomy of attacks in Section 3.

Post-processing approaches embed post-hoc watermarks into images. When watermarking AI-generated images, we apply such methods *after* the generation process. Post-processing watermarks are model-agnostic and applicable to any image. However, they sometimes introduce human-visible artifacts, compromising image quality. We review popular post-processing methods.

P1) Frequency-domain methods. These methods manipulate the representation of an image in some transform domain (Cox et al., 1996, ó Ruanaidh et al., 1996, O’Ruanaidh and Pun, 1997). The image transform can be a Discrete Wavelet Transform (DWT), Discrete Cosine Transform (DCT) (Cox et al., 2007), or SVD decomposition (Chang et al., 2005). These transformations have a range of invariance properties that make

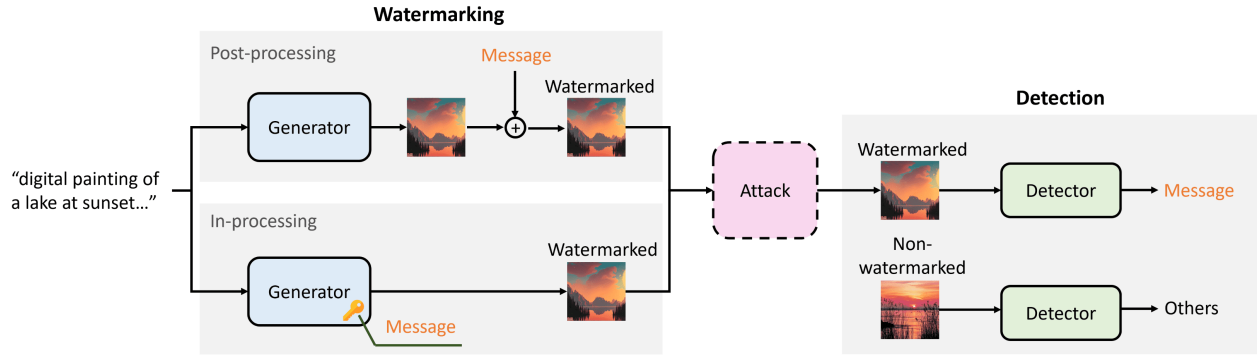


Figure 2. **An illustration of a robust watermarking workflow.** An AI company provides two services: (1) generate watermarked images, i.e., embed invisible messages, and (2) detect these messages when shown any of their watermarked images. There is an attack stage between the watermarking and detection stages. The watermarked images may experience natural distortions (e.g., compression, re-scaling) or manipulated by malicious users attempting to remove the watermarks. A robust watermarking method should still be able to detect the original message after an attack.

them robust to translation and resizing. The commercial implementation of Stable Diffusion (Rombach et al., 2022) uses DWTDC (Al-Haj, 2007) to watermark its generated images. However, many studies have shown that these watermarks are vulnerable to common image manipulations (Zhao et al., 2023a).

P2) Deep encoder-decoder methods. These methods rely on trained networks for embedding and decoding the watermark (Hayes and Danezis, 2017). Methods such as HiDDeN (Zhu et al., 2018) and RivaGAN (Zhang et al., 2019) learn an encoder to imprint a hidden message inside an image and a decoder (also called a detector) to extract the message. To train robust watermarks, RedMark (Ahmadi et al., 2020) integrates differentiable attack layers between the encoder and decoder in the end-to-end training process; RivaGAN (Zhang et al., 2019) employs an adversarial network to remove the watermark during training; StegaStamp (Tancik et al., 2020) adds a series of strong image perturbations between the encoder and decoder during training, resulting in watermarks which are robust to real-world distortions caused by photographing an image as it appears on a display.

P3) Others. There are other varieties of post-processing methods that do not fall into P1 or P2. SSL (Fernandez et al., 2022) embeds watermarks in self-supervised-latent spaces by shifting the image’s features into a designated region. DeepSigns (Rouhani et al., 2018) and DeepMarks (Chen et al., 2019) embed target watermarks into the probability density functions of weights and activation maps. Entangled watermarks (Jia et al., 2021) designs a reinforced watermark based on a target watermark and the task data.

In-processing methods adapt generative models to directly embed watermarks as part of the image generation process, substantially reducing or eliminating visible artifacts. With diffusion models presently dominating the field of image generation, a surge of in-processing approaches specific to these models has recently emerged. We categorize current work into three categories.

I1) Model modification. The entire model. This line of work inherits the encoder-decoder idea and bakes the encoder into the entire generative model. This is usually accomplished by watermarking training images with a pre-trained watermark encoder and decoder, then training or fine-tuning the generative model on these watermarked images (Lukas and Kerschbaum, 2023, Yu et al., 2021, Zeng et al., 2023). This type of method has been shown to work well on small models like guided diffusion, but suffers from the expensive training of large text-to-image generation models (Zhao et al., 2023b), making it inapplicable in practice.

Parts of the model. Stable Signature (Fernandez et al., 2023) follows the above two-stage training pipeline while only fine-tuning the decoder of the latent-diffusion model (LDM) (Rombach et al., 2022), leaving the diffusion component unchanged. This type of watermarker is much more efficient to train. By fine-tuning multiple latent decoders, the model can embed different messages into images.

Table 1. **Comparison of robustness evaluations with existing works.** For *categories of attacks*, D denotes distortions, R denotes image regeneration attacks, and A denotes adversarial attacks. *Reference image source* shows whether to use non-watermarked images in the evaluation and what is the source of those images. For the *number of quality metrics*, we use 8 in the paper but test 10 in total. *Joint test* means whether the performance and quality are jointly tested under a range of attack strengths. Our benchmark is the most comprehensive one, with a large scale of attacks, data, metrics, and more realistic evaluation setups.

Research Work	Num. of Attacks	Categories of Attacks	Num. of Datasets	Sample Size per Dataset	Non-watermarked Image Source	Performance Metric	Num. of Quality Metrics	Joint Test
StegaStamp Watermark (Tancik et al., 2020)	5	D	1	1000	-	bit accuracy	3	✗
Stable Signature Watermark (Fernandez et al., 2023)	12	D, R	1	5000	-	bit accuracy	3	✗
TreeRing Watermark (Wen et al., 2023)	6	D	2	1000	generate by same model	TPR@1%FPR	2	✗
Regeneration Attack (Zhao et al., 2023a)	10	D, R	2	500	-	bit accuracy	3	✗
Surrogate Model Attack (Saber et al., 2023)	2	R, A	1	2500	real images	AUROC	0	✗
Adaptive Attack (Lukas et al., 2023)	10	D, A	1	1000	real images	TPR@1%FPR	3	✗
WAVES (ours)	26	D, R, A	3	5000	real images	TPR@0.1%FPR	8 (10)	✓

The robustness of these two types of model modification critically relies on the robustness of the pre-trained encoder and decoder.

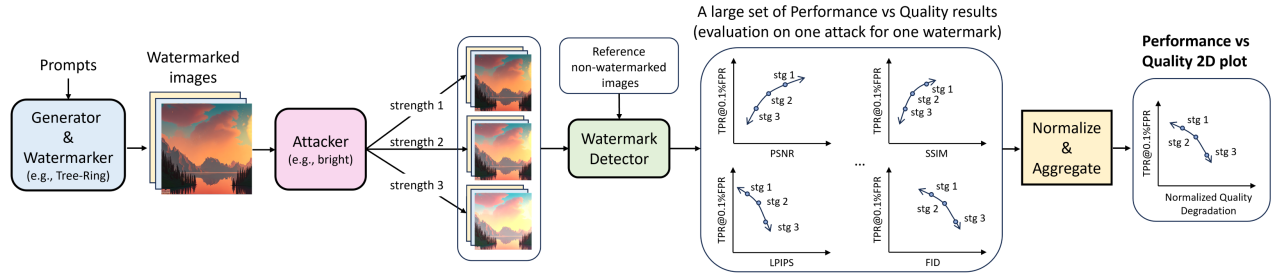
I2) Modification of a random seed. Tree-Ring (Wen et al., 2023), different from all the above methods, embeds a pattern into the initial noise vector used by a diffusion model for sampling. The pattern can be retrieved at detection time by inverting the diffusion process using DDIM (Song et al., 2020) as the sampler. This method does not require any training, can easily embed different watermarks, and is robust to many simple distortions and attacks. The robustness of Tree-Ring relies on the accuracy of the DDIM inversion.

2.2 Removing Watermarks

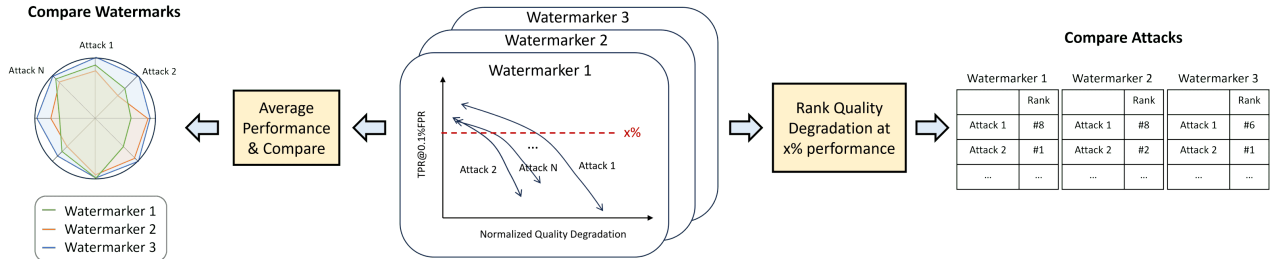
Robustness is an essential property of watermarks. Evaluations of robustness in existing literature focus on simple image distortions like rotation, Gaussian blur, etc. Recently, inspired by adversarial purification (Nie et al., 2022), Zhao et al. (2023a) and Saber et al. (2023) both find that regenerating images by noising and denoising images through a diffusion model or a VAE can effectively remove some watermarks. Saber et al. (2023) propose adversarial attacks based on a trained surrogate watermark detector. Lukas et al. (2023) also introduces adversarial attacks but requires the knowledge of the watermarking algorithm and a similar surrogate generative model. Jiang et al. (2023) studies white-box attacks and black-box query-based attacks. Some attacks are not possible in realistic scenarios where the attacker has only API access. Furthermore, existing evaluations use differing quality/performance metrics, making it difficult to compare the effectiveness between watermarking methods and between attacks.

3 Standardized Evaluation through WAVES

In this section, we introduce a comprehensive evaluation framework designed for rigorously stress-testing watermarks and facilitating comparative analysis among them. Firstly, we describe our evaluation workflow and the associated metrics. Subsequently, we detail our diverse set of 26 watermark attacks, spanning three distinct categories.



(a) Evaluation of a single attack on a watermarking method.



(b) Benchmarking watermarks and attacks.

Figure 3. **Evaluation workflow.** (a) Evaluation of a single attack on a watermarking method. We first attack watermarked images over a variety of strengths (also labeled ‘stg’). Then, we evaluate the detection performance (TPR@0.1%FPR) and a collection of image quality metrics such as PSNR, and plot a set of performance vs. quality plots. By normalizing and aggregating these quality metrics, we derive a consolidated 2D plot that represents the overall performance vs. quality for the evaluation. (b) Benchmarking watermarks and attacks. For each watermarking method, we plot all attacks on a unified performance vs. quality 2D plot to facilitate a detailed comparison. Based on this, we provide two additional analytical perspectives. We compare watermarks’ robustness through the averaged performance under different attacks. We evaluate attacks’ potency by ranking the quality at a specific performance threshold.

3.1 Standardized Evaluation Workflow and Metrics

We present a general message-based watermarking protocol, adaptable to AI detection and user identification, which generalizes most existing setups. This is followed by introducing key performance evaluation metrics to assess watermark robustness and the effectiveness of attacks in detection and identification scenarios. Furthermore, we employ a set of image quality metrics, along with a proposed normalized and aggregated quality metric, to facilitate comparative analysis of the impact of watermark methods and attacks on image quality.

3.1.1 General Watermarking Protocol

Applications of Invisible Image Watermarks. Originating from classical watermarks designed to protect creators’ intellectual property, invisible image watermarks have found broader applications in contemporary scenarios. With the rapid advancement of AI generative models, recent research primarily focuses on using invisible watermarks for two purposes: (1) **AI Detection** — detecting AI-generated images (Saberi et al., 2023), and (2) **User Identification** — identifying the user who generated the image for source tracking (Fernandez et al., 2023). The detection aspect is crucial for differentiating AI-generated images from others and safeguarding copyright, while identification is pivotal in scenarios where the model owner needs to track the source of an image, such as identifying a DALL·E user who created and spread the fake images. In this paper, we focus on these two applications.

Formulation of watermarking protocol. To fairly evaluate different watermark methods for varying applications, we start by formulating a general, message-based watermarking protocol which generalizes most existing setups. Let θ_G denote an image generator, \mathcal{M} the space of watermark messages, and \mathcal{X} the domain of images. We assume \mathcal{M} is a metric space with distance function $D(\cdot, \cdot)$. The choice of message space \mathcal{M} can

be very different depending on the watermarking algorithm: for Tree-Ring, messages are random complex Gaussians, while for the Stable Signature and StegaStamp, each message is a length- d binary string, where d denotes the length of the message. For watermarking algorithms following the encoder-decoder training approach, like Stable Signature and StegaStamp, the choice of message length d is fixed after training. Some methods, such as Tree-Ring, enjoy flexible message length at the time of injecting watermarks.

Watermark injection and recovery are often done by encoding a message m into the image, and later recovering the message m' , which may be an imperfect recovery, i.e. $m' \neq m$. Performance evaluation metrics of watermark detection and user identification that are statistically reliable and yet universally applicable across different watermarks, such as True Positive Rate at 0.1% False Positive Rate (TPR@0.1%FPR), will be introduced and compared with other metrics in Section 3.1.2.

Trade-Off between watermark performance and image quality. Watermark attacks, encompassing image augmentations and distortions, have the potential to significantly compromise image quality. This degradation can render the images effectively useless for unauthorized use or theft. Therefore, it is imperative to measure the degradation of image quality caused by watermark attacks. Comparisons of watermark attacks should therefore balance between watermark detection or identification efficacy and the extent of image quality degradation. *In this paper, we present all attack comparisons using Performance vs. Quality 2D plots.* To our best knowledge, we are the first to evaluate and compare watermark and attack methods based on the overall relation between performance and quality (i.e., the 2D plot), while most prior work focuses on the performance aspect and compare the performance and quality metrics independently. Our evaluation method provides a comprehensive perspective on the trade-off between performance and quality. We will introduce the image quality metrics in Section 3.1.3.

Evaluation workflow. Our evaluation methodology is designed to systematically assess the robustness of watermarking techniques against a spectrum of attacks. We begin by subjecting watermarked images to various attack methods and attack strengths, then employ the corresponding watermark detector to compare against reference non-watermarked images. As depicted in Figure 3, our evaluation process involves two equally-sized image datasets. The first set comprises watermarked images generated by the model θ_G . The second set consists of reference images, which are a mix of real images and AI-generated images from an entirely independent model and pipeline. Our evaluation rigorously mixes watermarked images from the model θ_G with non-watermarked images from independent sources. This ensures an unbiased and robust assessment, setting our method apart from and presenting a greater challenge than typical approaches in watermark research, such as those seen in Tree-Ring and Stable Signature studies. *Watermark performance metrics*, such as True Positive Rate at 0.1% False Positive Rate (TPR@0.1%FPR), are computed alongside a suite of *image quality metrics*. These results are normalized and aggregated to produce a consolidated 2D performance vs. quality plot, allowing us to benchmark watermark methods and attacks comprehensively. Our approach, WAVES, contrasts the individual attack analysis with a comparative view across multiple watermarks, providing a nuanced perspective on each method’s resilience.

Non-watermarked image datasets. We utilize three datasets for the non-watermarked reference images in our evaluation: **DiffusionDB**, **MS-COCO**, and **DALL-E3**, each comprising 5000 reference images and prompts. **DiffusionDB** represents a diverse collection from the DiffusionDB dataset (Wang et al., 2022), focusing on images generated from the Stable Diffusion (Rombach et al., 2022) models. **MS-COCO** is derived from the well-known Microsoft COCO detection challenge (Lin et al., 2014), featuring a wide range of everyday scenes and objects. **DALL-E3**¹ includes images from the DALL-E3 model, showcasing another popular diffusion model trained on substantially different data. These datasets provide a comprehensive range of image types and contexts, ideal for robust watermark evaluation. To view image examples of the three datasets, please see Figure 16. For comprehensive details on dataset preparation, please refer to Appendix C.1.

As shown in Table 1, our benchmark, WAVES, stands out by incorporating 26 diverse attacks across three categories and employing eight (out of 10 tested) quality metrics. This enables a joint evaluation of performance and quality degradation, distinguishing our work as the most extensive and realistic setup to date for watermark robustness evaluation.

¹The DALL-E3 dataset is hosted at <https://huggingface.co/datasets/laion/dalle-3-dataset>.

3.1.2 Performance Evaluation Metrics

To classify images as watermarked or non-watermarked, a good detector will often provide a p -value for the watermark detection, which measures the probability that the level of watermark strength observed in an image could happen by random chance. Rigorously, we have $p = P_m(D(\omega, m') < D(m, m') | H_0)$, where $D(\omega, m')$ is a dissimilarity metric between an arbitrary message $\omega \sim \mathcal{M}$ (selected uniformly at random) and recovered message m' from the image by the detector, and $D(m, m')$ denotes dissimilarity between the ground truth message m and the recovered message m' . H_0 denotes the null hypothesis that the image was generated without knowledge of the watermark (and therefore the recovered message is random). As in some prior work (Fernandez et al., 2023), one may set a threshold on the estimated p -value to determine the detection result. However, this approach makes it difficult to compare different watermark methods fairly. Even if we set the same p -value threshold on all watermark methods, the distinct choice of message space \mathcal{M} , message distribution P_m , and hypothesis test may differ. Therefore, we seek to evaluate watermark methods mainly using metrics that are independent of the choice of p -value threshold and statistical test.

We now describe several key evaluation metrics to assess the robustness of watermark methods and the potency of watermark attacks, specifically in detection and identification contexts. Our emphasis is on the fairness (independence from statistical testing and hyperparameters like p -value thresholds) and comprehensiveness (ability to reveal a watermark method’s fundamental capacity for encoding and recovering messages) of these metrics.

Performance metrics for AI detection. We can understand the AI detection problem as a standard binary classification, where metrics based on the receiver operating characteristic (ROC) curve, like the AUROC score, are independent of the choice of threshold. In AI-generated image applications, labeling non-watermarked images as watermarked (false positive) is particularly detrimental. As a result, strict control of false positive rate (FPR) is crucial. However, a high AUROC does not guarantee a high true positive rate (TPR) at low false positive rate (FPR) levels.

Our WAVES concentrates on the TPR at a specific low FPR, denoted as $\text{TPR}@x\% \text{FPR}$, as the primary performance metric. This aligns with a few recent studies (e.g., Fernandez et al. (2023), Wen et al. (2023)), but differs in our testing with a larger image dataset and a lower FPR threshold of 0.1%, compared to more common benchmarks like $\text{TPR}@1\% \text{FPR}$ in Tree-Ring. Choosing a lower FPR threshold is more challenging for watermark methods, and to our best knowledge, we are the first to evaluate watermark methods at such a low FPR threshold.

Performance metric for user identification. Similar to treating the AI detection setup as a binary classification problem, it is also natural to regard the user identification problem as a multi-class classification problem, while the number of classes is equal to the number of users. Classification is accomplished by evaluating the distance between the recovered message m' with each user’s message and assigning it to the user with the smallest distance. Our WAVES then measures the multi-class classification accuracy as the performance of user identification, which is the fraction of images that are correctly assigned to the user. More details on the efficient implementation of identification setup and more identification results are provided in Appendix D.1 and Appendix F.1 for reference.

3.1.3 Image Quality Metrics

No single image quality metric adequately captures all relevant aspects of generated images. Consequently, we utilize various metrics for a comprehensive comparison of attacks. Then we propose a normalized and aggregated quality metric to facilitate comparative analysis of watermark and attack methods.

Implementing diverse types of image quality metrics. WAVES has implemented over 10 metrics, categorized into 4 groups: (1) **Image similarities**, including Peak-Signal to Noise Ratio (PSNR), Structural Similarity Index (SSIM), and Normalized Mutual Information (NMI), which assess the pixel-wise accuracy after attack or distortions; (2) **Distribution distances** such as Frechet Inception Distance (FID) (Heusel et al., 2017) and a variant

based on CLIP feature space (CLIP-FID) (Kynkäänniemi et al., 2022); (3) **Perception-based metrics** like Learned Perceptual Image Patch Similarity (LPIPS) and the Watson’s perceptual distances (Watson-DFT) (Czolbe et al., 2020); (4) **Image quality assessments** including CLIP-Scores, aesthetics and artifacts scores (Xu et al., 2023), which quantify the changes in contextual deviations as well as aesthetic and artifact features. We implemented and experimented with all of these metrics, and found that the Watson-DFT and CLIP-Score cannot effectively reflect the image quality degradation of most proposed attacks. Therefore, we exclude these two metrics from our evaluation. We report the results with PSNR, SSIM, NMI, FID, CLIP-FID, LPIPS and changes in aesthetics and artifacts score (denoted by Delta Aesthetics and Delta Artifacts) in WAVES.

Normalization and aggregation of image quality metrics. The distinct characteristics of various image quality metrics pose challenges in defining a unified measure for image quality degradation. This complexity also complicates the establishment of a comprehensive score for attack or watermark methods, as it relies on the relationship between image quality and attack performance. Recognizing the necessity of a comprehensive score for ranking attack or watermark methods and constructing benchmarking leaderboards, WAVES proposes the design of a *normalized and aggregated quality metric*. This metric integrates eight representative quality metrics and a diverse array of attack methods.

Each of the 8 quality metrics under consideration has unique ranges and scales. To develop an overarching image quality metric that synthesizes these diverse inputs, normalization into a common interval is crucial. However, different quality metrics inherently reflect various aspects of image quality. For instance, some modified images may exhibit a high PSNR while maintaining a near-zero FID, illustrating the absence of a universal range for quality metrics. Instead of seeking a general equivalent interval, our focus is on specific applications, such as attacking invisible image watermarks. We aim to estimate an appropriate interval using a comprehensive set of examples. We define the normalized scale for each image quality metric by assigning the 10% quantile value of all attacked images (across 26 attack methods, over three watermark methods, and three datasets) as the 0.1 point, and the 90% quantile as the 0.9 point. Quality metrics are always ranked in ascending order of image degradation. The cumulative distribution functions (CDFs) of all eight image quality metrics across all attacked images are illustrated in Figure 17 in Appendix D.2. These plots reveal a roughly linear CDF between the 10% and 90% quantiles for all metrics, contrasting with the highly non-linear distribution outside this range, a characteristic of metrics like PSNR. Therefore, our attack-statistics-based normalization method yields a metric whose values carry equivalent significance across different quality metrics, defined by their quantiles in a large set of attacked watermarked images. After normalizing these eight image quality metrics, we aggregate them by averaging, defining this as the normalized (and aggregated) quality metric. This metric is extensively utilized in Section 4 to illustrate aggregated Performance vs Quality plots, watermark radar plots, and attack leaderboards. For detailed information on the design and definition of this normalized quality metric, please refer to Appendix D.2.

3.2 Stress-testing Watermarks

We comprehensively evaluate the robustness of three representative watermarking methods, Stable Signature (Fernandez et al., 2023), Stegstamp (Tancik et al., 2020), and Tree-Ring (Wen et al., 2023), with a wide range of attacks detailed in this section and summarized in Table 2. In Figure 4, we demonstrate the visual effects of various attacks on a tree-ring watermarked image.

3.2.1 Distortion Attacks

Watermarked images are often subjected to various distortions during internet transmission, such as compression, cropping, and adjustments in brightness and contrast. Consequently, it is essential for watermarks to demonstrate robustness against these common image distortions and manipulations.

While most research on image watermarking evaluates the resilience of methods against distortions, certain prior studies exhibit limitations in their testing approaches and methodologies. They either assess the



Figure 4. A visual demonstration of various adversarial, regeneration, and distortion attacks on a Tree-Ring watermarked image. **Figure (a)** is the base unattacked image. The base prompt, drawn from DiffusionDB, is “digital painting of a lake at sunset surrounded by forests and mountains,” along with further styling details.

Table 2. A taxonomy of all the attacks in our stress-testing set.

Category	Subcategory (prefix)	Description	Attack Names (suffix)	Requirements
Distortion	Single (Dist-)	Single distortion	-Rotation, -RCrop, -Erase, -Bright, -Contrast, -Blur, -Noise, -JPEG	-
	Combination (DistCom-)	Combination of a type of distortions	-Geo, -Photo, -Deg, -All	-
Regeneration	Single (Regen-)	A single VAE or diffusion regeneration	-Diff, -DiffP	DiffP requires user prompts
	Rinsing (Rinse-)	A multi-diffusion regeneration	-VAE, -KLVAE	KLVAE with bottleneck size 8 is grey-box
Adversarial	Embedding (grey-box) (AdvEmbG-)	Use the same VAE	-KLVAE8	grey-box
	Embedding (black-box) (AdvEmbB-)	Use other encoders	-RN18, -CLIP, -KLVAE16, -SdxVAE	-
	Surrogate detector attack (AdvCLS-)	Train a watermark detector	-UnWM&WM, -Real&WM, -WM1&WM2	need data and training

robustness of watermarks using only a single distortion operation or conduct tests exclusively with dramatic image degradations that indicate image tampering.

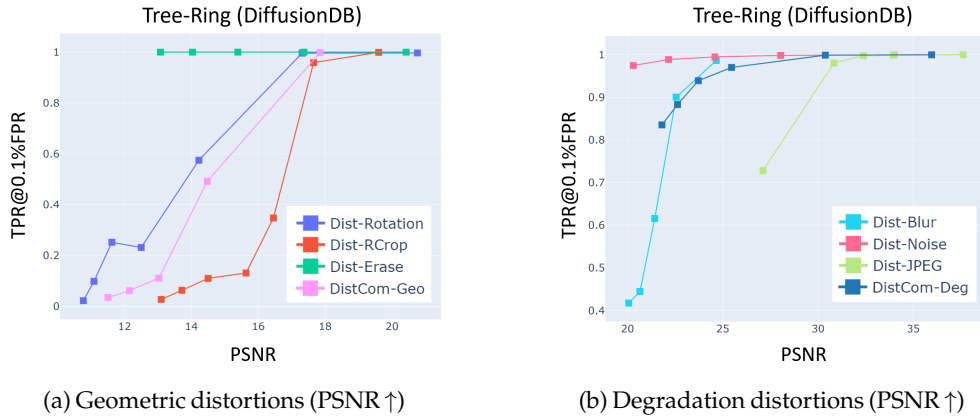


Figure 5. Distortions and their combinations. We combine three types of distortions: geometric, photometric, and degradation, both individually and collectively. By comparing quality-performance plots, we see combinations of distortions do not necessarily lead to better attacks.

In WAVES, we establish the following distortions within an acceptable quality threshold as our baseline:

1. **Geometric distortions:** rotation, resized-crop, and erasing;
2. **Photometric distortions:** adjustments in brightness and contrast;
3. **Degradation distortions:** Gaussian blur, Gaussian noise, and JPEG compression;
4. **Combo distortions:** combinations of geometric, photometric, and degradation distortions, both individually and collectively.

See Figure 5 for their comparison. Detailed setups for each are provided in the Appendix.

3.2.2 Image Regeneration Attacks

The diffusion purification (Nie et al., 2022, Saberi et al., 2023) attack passes an image through a pre-trained diffusion model, gradually noising and then denoising an image. The length (timesteps) of the diffusion process is typically short to retain image quality. Similarly, a pre-trained VAE may also be used to achieve the same effect, instead of compressing the image down to a latent space (likely different from the latent space of images produced by the black-box model), and then re-projecting it back into the fully-sized image space. Zhao et al. (2023a) classifies both diffusion purification and VAE attacks as *regeneration attacks*, a nomenclature we also adopt.

Different from existing literature (Nie et al., 2022, Saberi et al., 2023, Zhao et al., 2023a), we explore the effects of conducting *multi-regeneration*: an attack in which an image is repeatedly noised and denoised by a pre-trained diffusion model (taking advantage of the inexact inversion of a DDIM), which we also refer to as a **rinsing regeneration**. We also introduce two other simple, yet effective variations: prompted regeneration and mixed regeneration (rinse + VAE denoising), which are detailed in Appendix E.2.

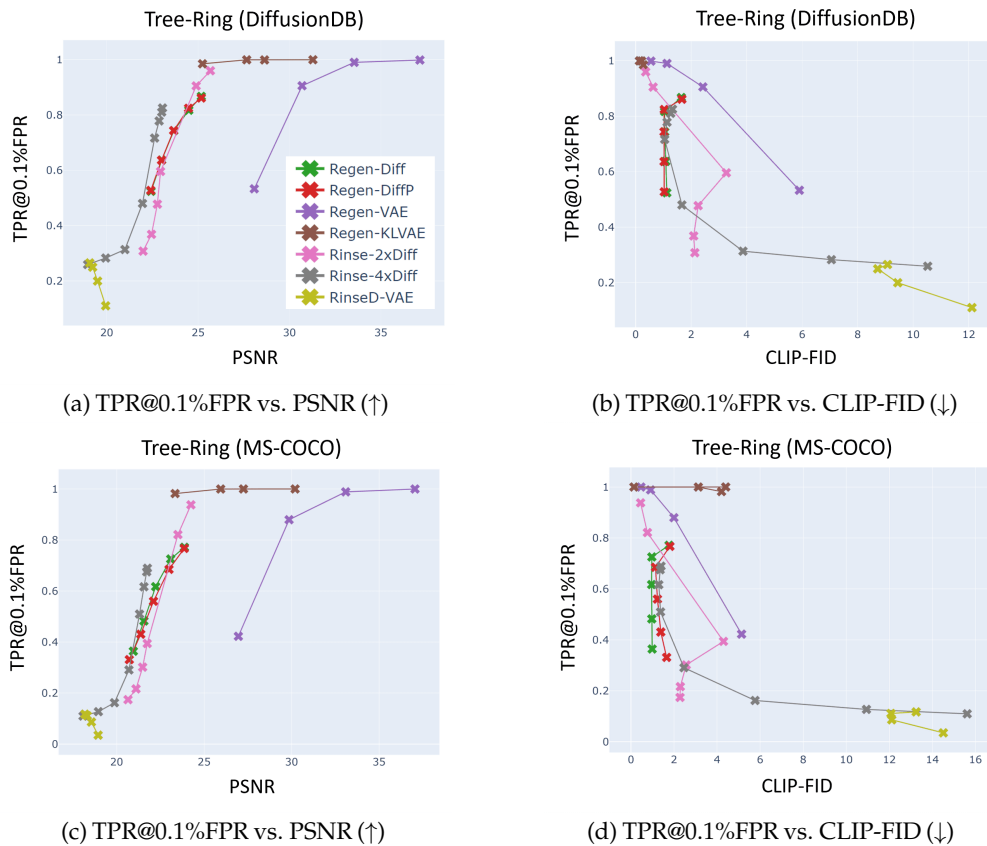


Figure 6. Regeneration attacks on the Tree-Ring watermark. Regen-Diff is a single diffusive regeneration and Rinse-[N]xDiff is a rinsing regeneration with N repeated diffusions; the strengths indicate the number of noising steps in each diffusion. Regen-VAE uses a pre-trained VAE (bmshj2018) (Ballé et al., 2018) from the CompressAI library with quality factor as strength and Regen-KLVAE uses pre-trained KL-loss VAEs from the CompVis (Kingma and Welling, 2022) with bottleneck size as strength. RinseD-VAE applies a VAE (bmshj2018) as a denoiser to Rinse-4xDiff attacked images. 2x rinsing and VAE regenerations are especially powerful against the Tree-Ring without extensively sacrificing image quality.

Figure 6 studies the effects of regeneration attacks on the Tree-Ring watermark. To simulate realistic diffusion regeneration attacks, we use a lower version diffusion model than the one used to generate the watermarked images (details in Appendix E.2). In contrast with the conclusions of Zhao et al. (2023a), the Tree-Ring watermark is not robust against a single regeneration attack (Regen-VAE, Regen-Diffusion). In particular, a

single deep diffusion regeneration or bmsj2018-VAE (Ballé et al., 2018) regeneration with low quality factor can significantly harm the TPR@0.1%FPR while maintaining reasonable CLIP FID. Rinsing regenerations significantly lower the TPR at the cost of markedly decreased image quality, although a 2x rinsing regeneration (Regen-2xDiffusion) strikes a balance between both low-TPR@0.1%FPR and high image quality.

In regards to the Stable Signature, Figure 11 and Table 3 concur with the analysis of Zhao et al. (2023a) – regeneration attacks (of either VAE or diffusive variety) are completely destructive and rinsing regenerations reiterate this phenomenon. The StegaStamp is similarly affected by regenerations, but only by diffusive attacks, including our novel rinsing and prompted regenerations.

3.2.3 Adversarial Attacks

Deep neural networks suffer from adversarial examples (Chakraborty et al., 2018, Ilyas et al., 2019) where small l_p perturbations to an image can fool a classifier. Watermark detectors are special image classifiers. As such, there are a range of adversarial attacks against them in a white-box setting (Jiang et al., 2023). It is interesting to see whether they are robust to adversarial attacks in black box settings that are more realistic for closed-source models. Here, we test two types of adversarial attacks.

(A) Embedding Attack. When watermark detection requires an image to pass through an embedding model that maps from the image space to the feature space, one can prevent detection by using a perturbation that disrupts the embedding. This is most effective when the attacker has white-box access to the embedding model. It is known that adversarial attacks sometimes transfer across models (Inkawhich et al., 2019), and have recently been used to attack Multimodal Large Language Models like Bard and GPT-4V (Dong et al., 2023). For this reason, we test whether attacks on standard off-the-shelf embedding models can transfer to the embeddings used by watermark detection.

Suppose we have an encoder $f: \mathcal{X} \rightarrow \mathcal{Z}$ that maps from image space to feature space. To remove watermarks, we optimize an adversarial image x_{adv} so that its embedding lies far from the original watermarked image x while ensuring the adversarial noise is in an l_∞ perturbation ball:

$$\max_{x_{adv}} \|f(x_{adv}) - f(x)\|_2, \quad \text{s.t. } \|x_{adv} - x\|_\infty \leq \epsilon.$$

We approximately solve this using the PGD (Madry et al., 2017) algorithm (see details in Appendix E.3.1), and hope the adversarial image transfers to real watermark detectors. We test three off-the-shelf encoders:

1. **(AdvEmbB-RN18)** uses a standard ResNet18 (He et al., 2016) pretrained from ImageNet (Deng et al., 2009). We attack the representation of the feature (pre-logit) layer.
2. **(AdvEmbB-CLIP)** uses CLIP (Radford et al., 2021), a pretrained Vision-Language Model which aligns the image representation with the text representation. We use the image encoder of CLIP to get embeddings. For watermarked images generated using text prompts, we investigate if such image-text-aligned features transfer to watermark detection.
3. **(AdvEmbG-KLVAE8)** uses KL-VAE, the autoencoder used in latent diffusion models (Rombach et al., 2022). We only use the encoder, which maps the image into the latent space while keeping all the semantic information. We first assume a grey-box setting where the adversary has access to the same KL-VAE (f8) used in the tested diffusion model. This is realistic since many proprietary models use public autoencoders. Then, we do ablation studies on KL-VAE (f16), which has a different architecture but is trained with the same data, and SDXL-VAE (Podell et al., 2023), an improved version of KL-VAE (f8). The last two attacks are denoted as **AdvEmbB-KLVAE16** and **AdvEmbB-SdxlVAE**.

We find that Stable Signature and StegaStamp are quite robust to embedding attacks. However, as shown in Figure 7, Tree-Ring is vulnerable to such attacks, especially when the adversary has access to the same

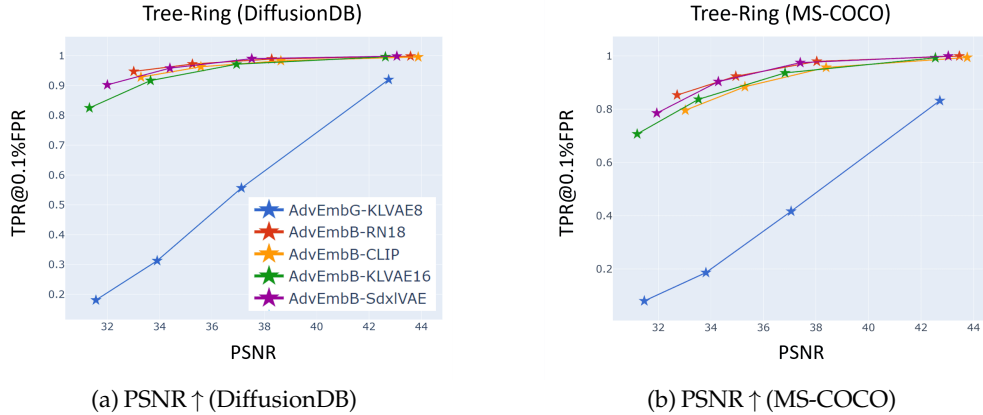
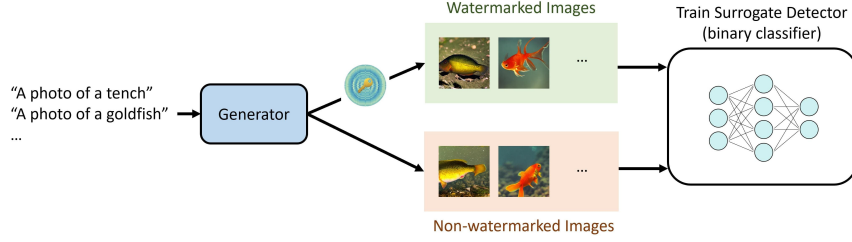


Figure 7. Adversarial embedding attacks on Tree-Ring. The attacks’ strengths are in [2/255, 4/255, 6/255, 8/255]. Tree-Ring is particularly vulnerable to embedding attacks when the adversary has access to the autoencoder being used.

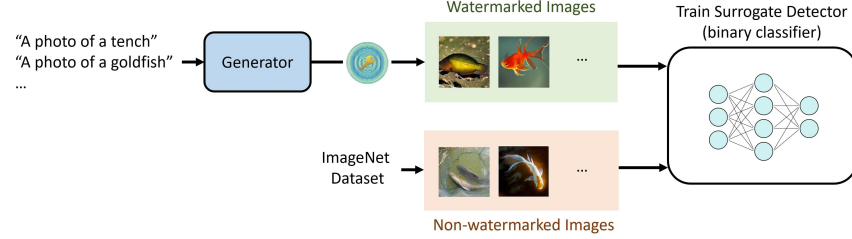
autoencoder being used. In this grey-box setting, TPR@0.1%FPR can degrade to nearly zero, effectively removing almost all the watermarks. This is because the detection process of Tree-Ring first maps the image to the latent representation through the encoder of KL-VAE (f8), then conducts inverse DDIM to retrieve the watermark. The embedding attack changes the latent representation severely; therefore, watermark retrieval becomes very difficult. When using similar but different VAEs, the effectiveness of the attacks becomes weaker, but they can still successfully remove some of the watermarks. KL-VAE (f16), the one trained from the same images, shows the best transferability. Embedding attacks based on CLIP can also remove some watermarks and perform strongly on MS-COCO. We speculate that this is because CLIP is trained on natural images similar to MS-COCO, leading to better transferability. The robustness of Stable Signature and StegaStamp is likely due to their detectors being trained independently from the generative models, making them quite distinct from standard classifiers and VAEs. As a result, our attempted attacks are ineffective in transferring to their detectors.

(B) Surrogate Detector Attack. Watermark detection relies on a detector that decodes the message from the watermarked image and then verifies it. An adversary could potentially obtain a large set of watermarked and non-watermarked images, and train a surrogate watermark detector. This detector can be attacked, and the attacks may transfer to the true watermark detector. Here, we consider the following settings for training the surrogate model with illustrations in Figure 8.

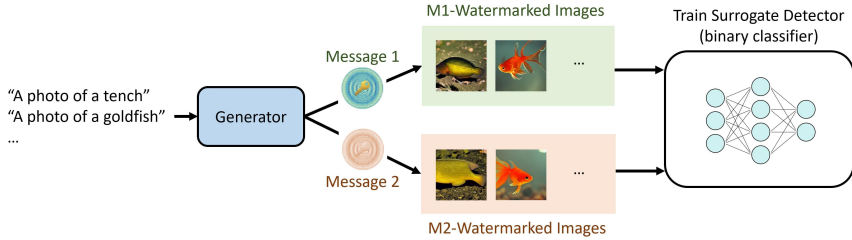
1. **(AdvCls-UnWM&WM)** Train surrogate detector with watermarked and non-watermarked images where both sets of images are generated by the victim generative model. This is the setting in [Saberi et al. \(2023\)](#). Note that this is technically a white-box threat model, as it assumes the attacker can obtain non-watermarked images from the model in question, which is not realistic for proprietary models.
2. **(AdvCls-Real&WM)** Train a surrogate detector with watermarked and non-watermarked images, where non-watermarked images are not sampled from the generative model. This setting is feasible when attacking a proprietary model. For non-watermarked images, we test on real natural images from ImageNet.
3. **(AdvCls-WM1&WM2)** Train a surrogate detector with only watermarked images. This approach is inspired by our findings from the first setting’s (AdvCls-UnWM-WM) analysis (refer to Appendix F.2), where we discovered that utilizing only watermarked images can fulfill the same goal of perturbing the latent features, alleviating the restrictions on the assumption. We collect watermarked images from two users, each employing a unique watermark message, using an identical set of prompts—a feasible scenario in practice. Then, we train a binary watermark message classifier.



(a) AdvCls-UnWM&WM. Train the surrogate watermark detector with watermarked and non-watermarked images, where images are all generated from the victim generator. This is an unrealistic setting for proprietary models since all their outputs are assumed to be watermarked.



(b) AdvCls-Real&WM. Train the surrogate watermark detector with watermarked and non-watermarked images, where non-watermarked images are sampled from the ImageNet dataset.



(c) AdvCls-WM1&WM2. Train the surrogate watermark message detector using watermarked images embedded with two different messages. If the system assigns a particular message to a user for identification purposes, the adversary can collect the training data from two users' outputs.

Figure 8. **Three settings for training the surrogate detector.** The Generator in the diagram is the victim generator under attack. We externalize the watermarking process in the diagram for simplicity, but it could be in-processing watermarks. After training the surrogate detectors, the adversary performs PGD attacks on them to flip the labels.

With the trained surrogate detector $f: \mathcal{X} \rightarrow \mathcal{Y}$, where $\mathcal{Y} = \{0,1\}$, the adversary conducts targeted attacks. Given an image x , the objective is to optimize the adversarial image x_{adv} such that the surrogate detector is misled into predicting the wrong label (i.e., flipped label) y_{target} ,

$$\min_{x_{adv}} L(f(x_{adv}), y_{target}), \quad \text{s.t.} \quad \|x_{adv} - x\|_{\infty} \leq \epsilon.$$

We minimize the cross-entropy loss to encourage such misclassification. In this way, the adversary can try to remove watermarks from the watermarked images or add watermarks to clean images in the first two settings, and can try to confuse the user identification and watermark detection in the last setting.

We train the surrogate detector by fine-tuning ResNet18. We use ImageNet images as the non-watermarked images in **AdvCls-Real&WM**, and generate watermarked images using ImageNet text prompts "A photo of a $\{class\ name\}$." The non-watermarked images in **AdvCls-UnWM&WM** are also generated using the same prompts with the same model but without adding watermarks. The watermarked images are generated using two different messages in **AdvCls-WM1&WM2** (see details in Appendix E.3.2). At test time, the adversary aims to remove watermarks from watermarked images.

As shown in Figure 9, Tree-Ring is vulnerable to this type of attack. In **AdvCls-UnWM&WM**, when the adversary can access the non-watermarked images, the attack based on the trained surrogate detector has good transferability and effectively removes watermarks. Interestingly, the same attacking method cannot be used to forge a watermark, which is usually called the spoofing attack, by adding a signal to a non-watermarked image (refer to Figure 21). We investigate the reasons behind this in Appendix F.2. It turns out that the watermark removal attack disturbs the entire latent space, not only the watermark, in order to remove the watermark (as shown in Figure 22). However, the spoofing attack fails as it perturbs the entire latent features without necessarily embedding the exact watermark.

In **AdvCls-Real&WM**, where the adversary cannot access the non-watermarked images generated by the same model, which is the case for proprietary models, the attack does not work. We speculate that the surrogate model learns not how to distinguish between watermarked and non-watermarked images but how to differentiate between real and generated images. To do so, the model uses a lot of features beyond simply the watermark.

We successfully attack the Tree-Ring with only watermarked images in **AdvCls-WM1&WM2**. Our new attack trains a surrogate model to classify watermarked images with two different watermark messages. As illustrated in Figure 23, similar to our findings in the first setting, the surrogate model fails to locate watermarks accurately. However, it learns the mapping from the image space to the latent feature space of the generator. Consequently, a PGD attack can disrupt the entire latent features including the watermark, thereby achieving the effect of removing the watermark. This attack operates on the same working mechanism as the first attack, but the adversary only needs images with watermarks, rendering a strong and realistic attack. In the user identification task, as depicted in Figure 24, this attack cannot always mislead the detector into identifying User1’s watermarked images as belonging to User2. Instead, User1’s images are often misattributed to other users, mainly due to the imprecise perturbation. This trend is more pronounced in systems with a larger user base. Conversely, in systems with fewer users and under more intense attack conditions, targeted identification is possible.

The Stable Signature and StegaStamp are robust to these attacks (as shown in Figure 12). Even in **AdvCls-UnWM&WM**, when the surrogate classifier’s testing accuracy is near 100%, the attack cannot mislead the true detector, meaning the adversarial examples do not transfer. It is possible that there are spurious features that can also help to classify watermarked and non-watermarked images, differing from the features used by the true detector.

4 Benchmarking Results and Analysis

The WAVES framework illuminates several hidden vulnerabilities of popular watermarking strategies. In this section, we benchmark the watermarks and attacks according to the workflow in Figure 3. We focus on the detection setup first and then discuss the identification results. In the end, we provide valuable insights and suggestions to the community.

4.1 Processing Results

A set of Performance vs. Quality 2D plots show the detailed evaluation results. We evaluate 3 watermarking methods under the 26 attacks, and report results across 3 datasets in Figure 25 to Figure 30. The quality of

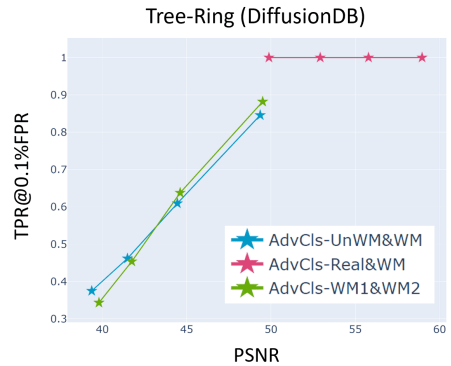


Figure 9. Adversarial surrogate detector attack on Tree-Ring. **AdvCls-UnWM&WM** is an unrealistic setting where non-watermarked images from the victim generative model are needed. With the newly proposed attack **AdvCls-WM1&WM2**, the adversary only needs watermarked images but can still train a surrogate model to remove watermarks.

images post-attack is evaluated using 8 metrics and the detection performance of 3 methods is measured by TPR@0.1%FPR.

Different quality metrics yield similar ranking of attacks. Despite measuring different aspects of image quality, we observe that eight quality metrics consistently produce similar rankings for attacks, as illustrated in Figure 10. Since a strong attack should remove the watermark without sacrificing the image quality, we rank attack potency by ranking the post-attack quality, from best to worst, at a frozen performance threshold (e.g., TPR@0.1%FPR=0.95). Upon comparing the rankings derived from different quality metrics, we find that the variations in rank order are minimal. Consequently, we aggregate these metrics into a single, unified quality metric.

Unified Performance vs. Quality degradation 2D plots. We first set the “standardized” 0.1 and 0.9 points for each metric according to the distribution of measured values (as depicted in Figure 17). Subsequently, every metric’s value is normalized to predominantly fall within the [0.1,0.9] range of the normalized quality metric (the detailed methodology is provided in Appendix D.2). We average these normalized quality scores to derive the *Normalized Quality Degradation*, with lower scores indicating lesser quality degradation caused by attacks, which is preferred. Furthermore, we aggregate the results across three distinct datasets. The Performance vs. Quality degradation 2D plots, as shown in Figure 11, visualize the unified evaluation results for each watermarking method. We use unified Performance vs. Quality degradation 2D plots to benchmark watermarks and attacks in the following sections.

Image Quality Ranks at TPR@0.1%FPR=0.95

	PSNR	SSIM	NMI	FID	CLIP-FID	LPIPS	Aesth	Artifacts	Rank
DistComGeo	14.76	0.4	1.12	5.96	4.88	0.21	1.12	-0.46	8
DistComPhoto	NA	NA	NA	NA	NA	NA	NA	NA	9
DistComDeg	22.3	0.61	1.2	23.46	11.19	0.48	1.21	-0.46	7
RegenDiff	23.87	0.73	1.2	7.64	1.77	0.11	0.32	-0.19	6
Rinse2xDiff	24.25	0.76	1.22	3.18	0.45	0.09	0.25	-0.04	5
AdvEmbCLIP	38.39	0.95	1.48	4.49	66.23	0.04	0.58	-0.26	4
AdvEmbKLVAE8	42.71	0.98	1.62	1.69	0.7	0.03	0.15	-0.06	3
AdvEmbKLVAE16	36.82	0.93	1.49	3.69	1.52	0.07	0.35	-0.13	2
AdvCLSWM1-WM2	49.41	1.0	1.69	0.34	0.23	0.0	0.11	-0.05	1

Figure 10. **Ranking attacks with different quality metrics** on DiffusionDB images watermarked by Tree-Ring. Attack potency is ranked by image quality at 0.95 TPR@0.1%FPR. Colors indicate the ranks (1=best, 9=worst), and values show the measured quality. We use 'NA' to label an attack if its attack curve lies entirely above TPR=0.95; the attack is automatically ranked last.

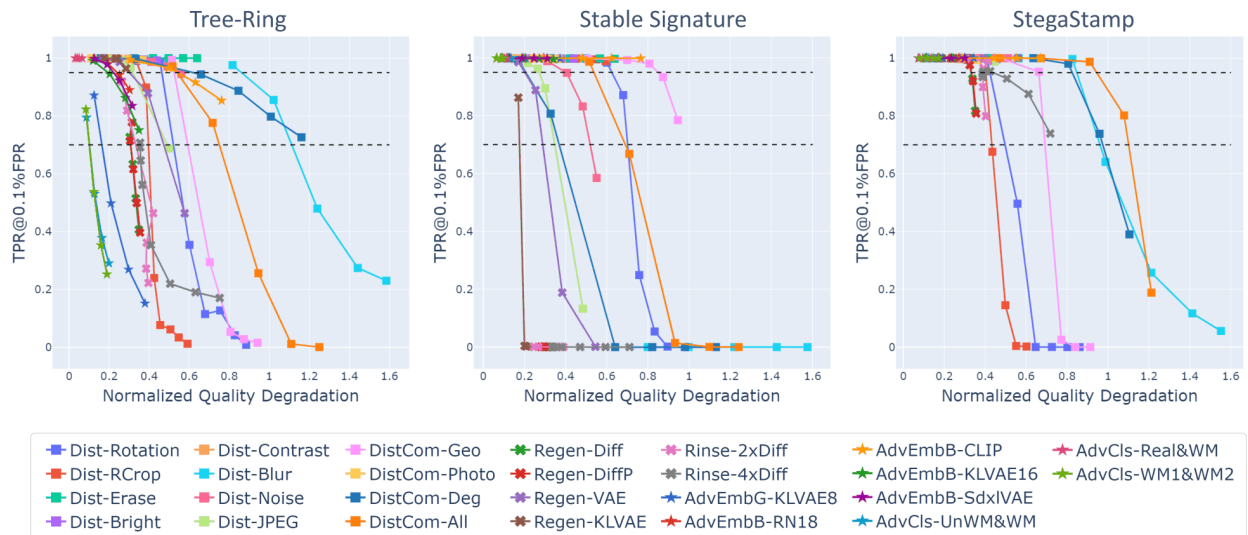


Figure 11. **Aggregated performance vs. quality degradation 2D plots under detection setup.** We evaluate each watermarking method under various attacks. Two dashed lines show the thresholds used for ranking attacks.

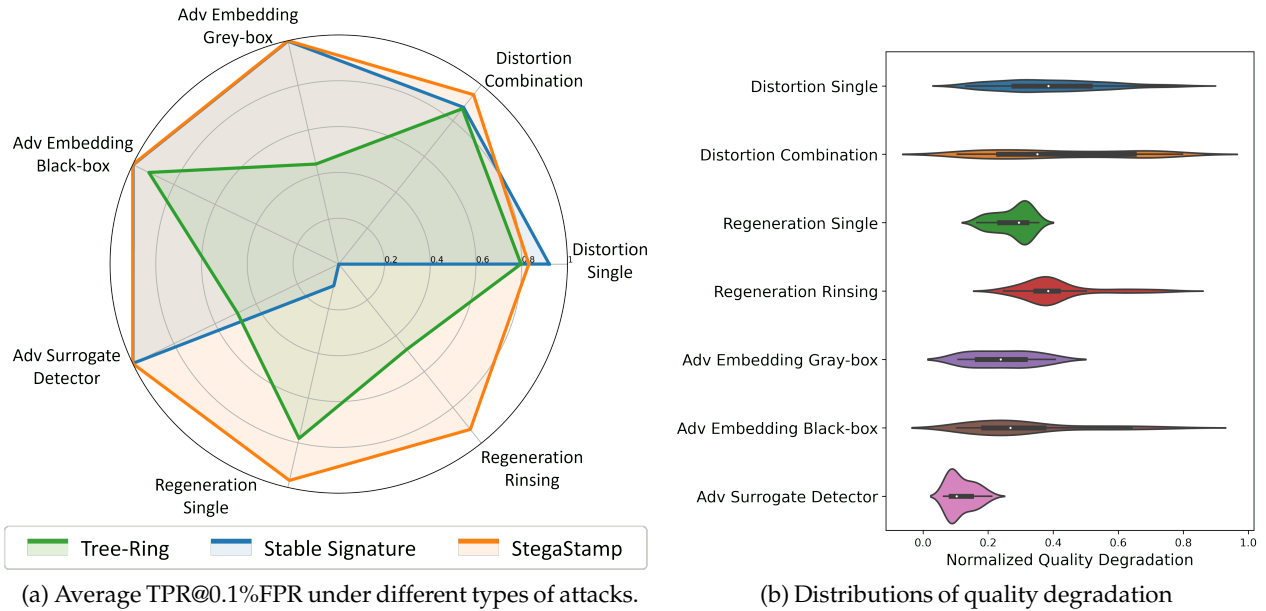


Figure 12. (a) Comparing the detection performance (i.e., TPR@0.1\%FPR) of Stable Signature, StegaStamp, and Tree-Ring watermarks via WAVES. We compute the Average TPR@0.1\%FPR across all strength levels and further averaged this metric across different attacks and datasets. Lower Average TPR@0.1\%FPR indicates higher vulnerability of the watermark to a certain type of attack. (b) Considering that various attacks result in differing levels of quality degradation, we also present the distribution of quality degradation for each type of attack. Lower quality degradation is preferred.

4.2 Benchmarking Watermark Robustness

We aggregate results in 2D plots into Figure 12, providing a high-level overview of watermarks’ robustness. We first select effective attacks and group them into seven attack categories (same as categories in Table 2): *Distortion Single*, *Distortions Combination*, *Regeneration Single*, *Regeneration Rinsing*, *Adv Embedding Grey-box*, *Adv Embedding Black-box*, and *Adv Surrogate Detector*. Attacks considered are specified in Appendix D.3. Then, we compute the Average TPR@0.1\%FPR across all practical strength levels that cause quality degradation less than 0.8, and across all attacks in each category. We compare the robustness of three watermarking methods in Figure 12a where the Average TPR@0.1\%FPR represents the robustness of watermarks under each type of attack. The area covered indicates the overall robustness. Figure 12b shows the distribution of quality degradation for each type of attack. This is to remind readers that even though some attacks are effective, they might also lead to reduced image quality.

WAVES provides a clear comparison of watermarks’ robustness and reveals undiscovered vulnerabilities. The radar plot comparison in Figure 12a reveals that StegaStamp occupies the largest area, signaling its exceptional robustness. Tree-Ring follows suit with a smaller area, and Stable Signature occupies the least space. Interestingly, different watermarking methods exhibit vulnerabilities to different types of attacks. Tree-Ring is mostly vulnerable to adversarial attacks, especially to grey-box embedding attack and surrogate detector attack proposed in this paper. Stable Signature is vulnerable to almost all regeneration attacks. All three watermarks maintain a relative robustness against distortions. Furthermore, as observed in Figure 12b, adversarial attacks generally cause less quality degradation, highlighting their potency against Tree-Ring watermarks.

4.3 Benchmarking Attacks

In addition to benchmarking watermarks, WAVES also facilitates the analysis from the perspective of attacks. Table 3 provides a leaderboard of individual attacks. A strong attack should result in low post-attack detection

performance while simultaneously preserving image quality for practical uses. Therefore, we benchmark attacks according to both performance and quality degradation. Based on three Performance vs. Quality 2D plots in Figure 11, we first select two performance thresholds, $\text{TPR}@0.1\%\text{FPR}=0.95$ and $\text{TPR}@0.1\%\text{FPR}=0.7$, ensuring intersections with most attack curves. Then, we calculate the quality degradation for each attack at these two performance thresholds, denoted as $\text{Q}@0.95\text{P}$ and $\text{Q}@0.7\text{P}$. Given that some attack curves do not intersect with either threshold, we also compute each attack’s average performance and quality degradation across all strengths, termed as Avg P and Avg Q. We report these metrics — $\text{Q}@0.95\text{P}$, $\text{Q}@0.7\text{P}$, Avg P, and Avg Q — for attack comparison. Based on them, we also provide a ranking of 26 attacks for each watermarking method for reference. During this ranking process, we incorporate a 0.01 buffer for both P and Q, meaning that if the difference between any two values is less than 0.01, they are considered a tie in terms of ranking.

The potency of attacks varies across different watermarks. In Table 3, we note considerable variability in attack performance across different watermarking methods. The $\text{Q}@0.95\text{P}$ and $\text{Q}@0.7\text{P}$ metrics offer a nuanced comparison of attacks, while Avg P and Avg Q provide a comprehensive view of each attack’s overall potency and its impact on image quality. Examining these four metrics alongside the indicative rankings, our findings highlight the specific vulnerabilities of each watermarking method to certain individual attacks. Notably, AdvCls-UnWM&WM, AdvCls-WM1&WM2, and AdvEmbG-KLVAE8 show remarkable effectiveness against Tree-Ring. In contrast, attacks like Regen-Diff and Regen-DiffP demonstrate greater potency against Stable Signature. While regeneration attacks exhibit some effect on StegaStamp, they do not significantly reduce average detection performance; however, some distortion attacks cause a notable decrease in detection performance, albeit with considerable quality degradation. There is no single attack that consistently outperforms others across different watermarking methods, yet regeneration attacks exhibit some

Table 3. Comparison of attacks across three watermarking methods under the detection setup. Q denotes the normalized quality degradation, and P denotes the performance as derived from Figure 11. $\text{Q}@0.95\text{P}$ measures quality degradation at a 0.95 performance threshold where "inf" denotes cases where all tested attack strengths yield performance above 0.95, and "-inf" where all are below. A similar notation applies to $\text{Q}@0.7\text{P}$. Avg P and Avg Q are the average performance and quality over all the attack strengths. The lower the performance and the smaller the quality degradation, the stronger the attack is. For each watermarking method, we rank attacks by $\text{Q}@0.95\text{P}$, $\text{Q}@0.7\text{P}$, Avg P, Avg Q, in that order, with lower values (↓) indicating stronger attacks. The top 5 attacks of each watermarking method are highlighted in red.

Attack	Tree-Ring					Stable Signature					StegaStamp				
	Rank	$\text{Q}@0.95\text{P}$	$\text{Q}@0.7\text{P}$	Avg P	Avg Q	Rank	$\text{Q}@0.95\text{P}$	$\text{Q}@0.7\text{P}$	Avg P	Avg Q	Rank	$\text{Q}@0.95\text{P}$	$\text{Q}@0.7\text{P}$	Avg P	Avg Q
Dist-Rotation	11	0.464	0.521	0.375	0.648	12	0.624	0.702	0.594	0.650	5	0.423	0.498	0.357	0.616
Dist-RCrop	18	0.592	0.592	0.332	0.463	24	inf	inf	0.995	0.461	6	0.602	0.602	0.540	0.451
Dist-Erase	26	inf	inf	1.000	0.490	25	inf	inf	0.998	0.489	25	inf	inf	1.000	0.483
Dist-Bright	25	inf	inf	0.997	0.304	23	inf	inf	0.998	0.305	22	inf	inf	0.998	0.317
Dist-Contrast	22	inf	inf	0.998	0.243	20	inf	inf	0.998	0.243	17	inf	inf	0.998	0.231
Dist-Blur	20	0.861	1.112	0.563	1.221	5	-inf	-inf	0.000	1.204	9	0.848	0.962	0.414	1.198
Dist-Noise	16	0.548	inf	0.980	0.395	8	0.402	0.520	0.870	0.390	24	inf	inf	1.000	0.360
Dist-JPEG	12	0.499	0.499	0.929	0.284	9	0.485	0.485	0.793	0.284	21	inf	inf	0.998	0.263
DistCom-Geo	13	0.525	0.593	0.277	0.768	13	0.850	inf	0.937	0.767	7	0.663	0.693	0.396	0.733
DistCom-Photo	22	inf	inf	0.998	0.242	20	inf	inf	0.998	0.243	17	inf	inf	0.998	0.239
DistCom-Deg	19	0.620	inf	0.892	0.694	7	0.206	0.369	0.300	0.679	8	0.826	0.975	0.852	0.664
DistCom-All	14	0.539	0.751	0.403	0.908	11	0.538	0.691	0.334	0.900	10	0.945	1.101	0.795	0.870
Regen-Diff	5	-inf	0.307	0.612	0.323	1	-inf	-inf	0.001	0.300	1	0.331	inf	0.943	0.327
Regen-DiffP	4	-inf	0.307	0.601	0.327	1	-inf	-inf	0.001	0.303	1	0.333	inf	0.940	0.329
Regen-VAE	17	0.578	0.578	0.832	0.348	10	0.545	0.545	0.516	0.339	23	inf	inf	1.000	0.343
Regen-KLVAE	22	inf	inf	0.990	0.233	6	-inf	0.176	0.217	0.206	17	inf	inf	1.000	0.240
Rinse-2xDiff	6	-inf	0.333	0.510	0.357	3	-inf	-inf	0.001	0.332	4	0.391	inf	0.941	0.366
Rinse-4xDiff	7	-inf	0.355	0.443	0.466	4	-inf	-inf	0.000	0.438	3	0.388	inf	0.909	0.477
AdvEmbG-KLVAE8	3	-inf	0.164	0.448	0.253	20	inf	inf	0.998	0.249	17	inf	inf	1.000	0.232
AdvEmbB-RN18	10	0.241	inf	0.953	0.218	17	inf	inf	0.999	0.212	14	inf	inf	1.000	0.196
AdvEmbB-CLIP	15	0.541	inf	0.932	0.549	26	inf	inf	0.999	0.541	25	inf	inf	1.000	0.488
AdvEmbB-KLVAE16	8	0.195	inf	0.888	0.238	19	inf	inf	0.997	0.233	14	inf	inf	1.000	0.206
AdvEmbB-SdxlVAE	9	0.222	inf	0.934	0.221	17	inf	inf	0.998	0.219	14	inf	inf	1.000	0.204
AdvCls-UnWM&WM	1	-inf	0.102	0.499	0.145	14	inf	inf	0.999	0.101	11	inf	inf	1.000	0.101
AdvCls-Real&WM	21	inf	inf	1.000	0.047	14	inf	inf	0.998	0.092	11	inf	inf	1.000	0.106
AdvCls-WM1&WM2	1	-inf	0.101	0.492	0.139	14	inf	inf	0.999	0.084	13	inf	inf	1.000	0.129

level of effectiveness against all three methods. This significant variation in attack effectiveness emphasizes the imperative for diverse and watermark-tailored defensive strategies in the realm of image watermarking.

4.4 Benchmarking Results for User Identification

In this subsection, we present the user identification results. We evaluate the user identification according to the method introduced in Section 3.1. The only difference between the evaluations of identification and detection is that we use identification accuracy as the performance metric here. Our analysis encompasses scenarios with varying user numbers: 100, 1,000, and 1 million, to simulate diverse real-world conditions. Employing the same evaluation procedure, we derive the unified Performance vs. Quality degradation 2D plots in Figure 13, radar plots for comparing watermarks in Figure 14, and leaderboard of attacks under identification setup in Table 5.

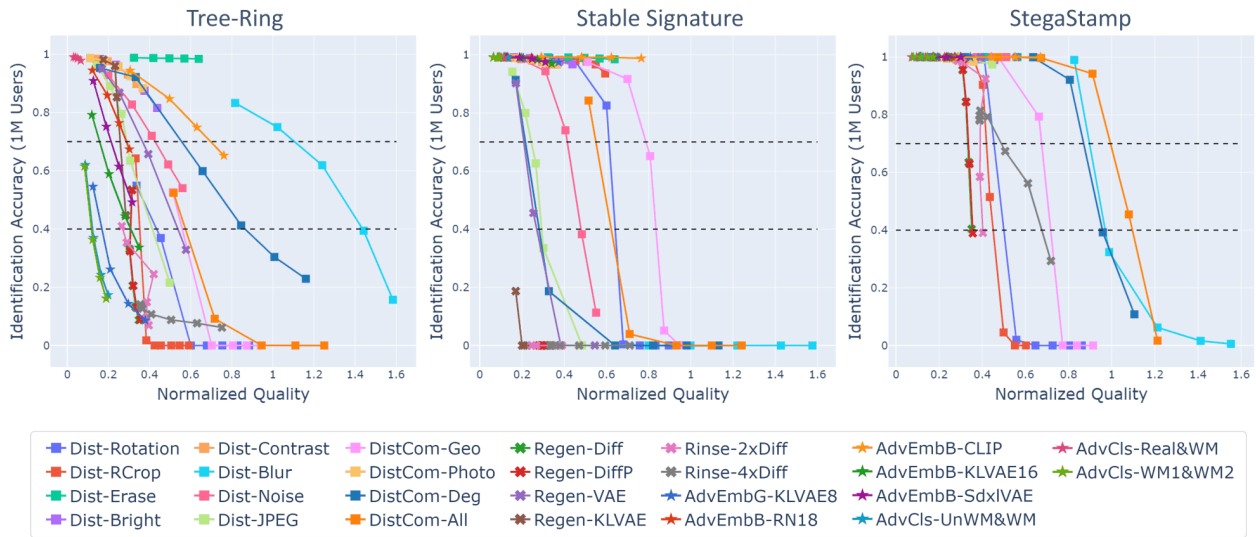


Figure 13. Aggregated performance vs. quality degradation 2D plots under identification setup (one million users). We evaluate each watermarking method under various attacks. Two dashed lines show to thresholds used for ranking attacks.

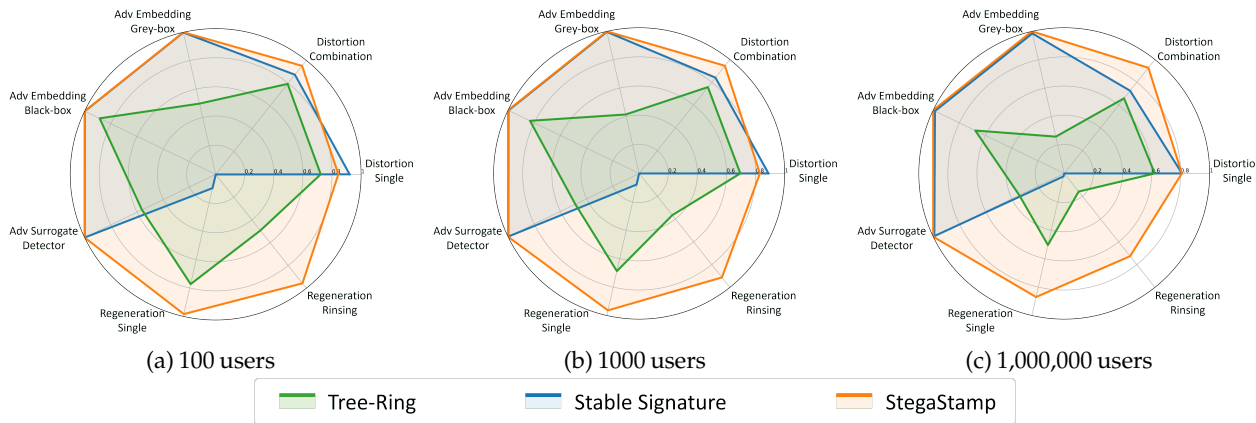


Figure 14. Comparing the identification performance (i.e., accuracy) of Stable Signature, StegaStamp, and Tree-Ring watermarks via WAVES. We simulate identification tasks with total user counts of 100, 1,000, and 100,000.

Identification results mirror findings from detection, highlighting similar trends in watermark robustness and attack potency. As shown in Figure 14 and Table 5, the comparison between the robustness of the

three watermarking methods and the comparison of the attack potency align closely with insights from the detection setup. This is largely due to both setups depending on accurate watermark message decoding, and almost all attacks considered in this paper being generally perturbing the images. Additionally, we observe that the vulnerability of watermarks to attacks escalates with an increasing user base. This is particularly noticeable in cases where certain attacks already have a strong destructive effect on watermark detection. Given that the identification process requires higher accuracy in message decoding, the vulnerability of identification correspondingly intensifies with the increasing number of users. Consequently, insights gained from detection scenarios are often applicable to identification, especially when attacks are not identification-specific. Watermarking methods should be particularly vigilant about attacks that demonstrate significant vulnerability during detection. It is possible that future attacks may be tailored for user identification, as exemplified by AdvCls-WM1&WM2 in this paper. Watermarking methods may need to evolve to potentially address vulnerabilities in both detection and identification in the future.

4.5 Summary of Takeaway Messages

We summarize the takeaway messages in the following.

WAVES provides a standardized framework for benchmarking watermark robustness and attack potency. WAVES can evaluate both detection and identification tasks. It unifies the quality metrics and assesses attack potency against both performance degradation and quality degradation. The Performance vs. Quality 2D plots allow for a comprehensive analysis of various watermarking methods, and different attack techniques in one unified framework. WAVES employs more than twenty attacks for stress-testing, revealing previously undetected vulnerabilities of popular watermarks.

Different watermarking methods have different vulnerabilities. Our analysis reveals significant differences in watermark vulnerabilities against attacks. Specifically, Tree-Ring is more vulnerable to adversarial attacks, which generally cause less quality degradation, while Stable Signature is susceptible to most regeneration attacks. This diversity in vulnerabilities highlights the imperative for watermarking methods to specifically strengthen their weakest areas.

Avoid using publicly available VAEs. WAVES reveals that when the diffusion model uses a publicly available VAE, in our case the KL-VAE (f8), an adversarial embedding attack using the same VAE can perturb the image’s latent feature without changing much of the image, defeating the Tree-Ring watermark easily. Additionally, if the diffusion model watermarked by Stable Signature uses a public VAE’s encoder, it’s vulnerable to regeneration attacks using that VAE. This occurs because the watermark, embedded in the model’s decoder, is bypassed when the public VAE replicates the latent representation but projects it back to pixel space using a non-watermarked decoder. Today’s proprietary image generators typically train the most crucial part themselves - the latent diffusion model - and use a public pre-trained VAE. It is known that DALL·3 uses a public KL-VAE². If it adopts watermarking methods similar to Tree-Ring or Stable Signature, it is quite susceptible to being attacked. Our findings call for attention to this severe vulnerability that may already exist.

The robustness of StegaStamp potentially illuminates a path for future robust watermarks. In our evaluation, StegaStamp emerges as the most robust one, likely due to its training approach. The StegaStamp (Tancik et al., 2020) watermark is used in the physical world, requiring high robustness. The watermark encoder and decoder are trained with a series of distortions reflecting real-world scenarios, which significantly strengthens the robustness of the watermark detector. However, it’s important to recognize the potential trade-off between watermark robustness and quality. While StegaStamp, as a post-processing method, exhibits high robustness, it may introduce artifacts. In contrast, this might not pose a problem for in-processing watermarks. Therefore, in-processing watermarks could still benefit from incorporating augmentation or adversarial training during their training phase.

²According to <https://cdn.openai.com/papers/dall-e-3.pdf>.

5 Conclusion

In this work, we comprehensively assess the robustness of several popular watermarking techniques. Our framework, WAVES, uses a battery of attacks to degrade a watermark. The potency of an attack is jointly judged against two metrics: detection/identification probability of the watermark and quality of the image after the attack. We provide a taxonomy, categorization, and ranking of over 20+ styles of attack on the DiffusionDB, MSCOCO, and DALLE-3 datasets. In particular, our normalized ranking of an attack’s viability aggregates many popular perceptual metrics. Our analysis highlights the vulnerabilities of existing watermarking strategies. WAVES can serve as a practical field guide to the design and evaluation of any watermarking algorithm.

Limitations. We only stress-test the Tree-Ring, Stable Signature, and Stegastamp watermarking algorithms. We curated these watermarks for WAVES after an extensive literature review indicated these three techniques to be the most powerful and practical candidates for deployment in the wild. However, we emphasize our framework is extensible to any watermarking method. Additionally, our attack ranking method relies on author-selected TPR thresholds and image quality metrics that we believe will fairly capture attack potency based on existing literature and experimental studies. The use of other quality metrics (MSE, Watson-DFT, etc.) and differing TPR thresholds may affect attack rankings.

Acknowledgments

We thank Souradip Chakraborty and Amrit Singh Bedi for insightful discussions.

An, Ding, Rabbani, Deng, Xu, Zhu, and Huang are supported by National Science Foundation NSF-IIS FAI program, DOD-ONR-Office of Naval Research under award number N00014-22-1-2335, DOD-AFOSR-Air Force Office of Scientific Research under award number FA9550-23-1-0048, Capital One and JP Morgan faculty fellowships.

Wen and Goldstein are supported by the ONR MURI program, the AFOSR MURI program, the National Science Foundation (IIS-2212182), the NSF TRAILS Institute (2229885), Capital One Bank, the Amazon Research Award program, and Open Philanthropy.

References

- Mahdi Ahmadi, Alireza Norouzi, Nader Karimi, Shadrokh Samavi, and Ali Emami. Redmark: Framework for residual diffusion watermarking based on deep networks. *Expert Systems with Applications*, 146:113157, 2020.
- Ali Al-Haj. Combined dwt-dct digital image watermarking. *Journal of computer science*, 3(9):740–746, 2007.
- Johannes Ballé, David Minnen, Saurabh Singh, Sung Jin Hwang, and Nick Johnston. Variational image compression with a scale hyperprior. In *6th International Conference on Learning Representations, ICLR 2018, Vancouver, BC, Canada, April 30 - May 3, 2018, Conference Track Proceedings*. OpenReview.net, 2018.
- Anirban Chakraborty, Manaar Alam, Vishal Dey, Anupam Chattopadhyay, and Debdeep Mukhopadhyay. Adversarial attacks and defences: A survey. *arXiv preprint arXiv:1810.00069*, 2018.
- Chin-Chen Chang, Piyu Tsai, and Chia-Chen Lin. Svd-based digital image watermarking scheme. *Pattern Recognition Letters*, 26(10):1577–1586, 2005.
- Huili Chen, Bitar Darvish Rouhani, Cheng Fu, Jishen Zhao, and Farinaz Koushanfar. Deepmarks: A secure fingerprinting framework for digital rights management of deep learning models. In *Proceedings of the 2019 International Conference on Multimedia Retrieval*, pages 105–113, 2019.

- Ingemar Cox, Matthew Miller, Jeffrey Bloom, Jessica Fridrich, and Ton Kalker. Digital watermarking and steganography. Morgan kaufmann, 2007.
- Ingemar J Cox, Joe Kilian, Tom Leighton, and Talal Shamoan. Secure spread spectrum watermarking for images, audio and video. In Proceedings of 3rd IEEE international conference on image processing, pages 243–246. IEEE, 1996.
- Steffen Czolbe, Oswin Krause, Ingemar Cox, and Christian Igel. A loss function for generative neural networks based on watson’s perceptual model. Advances in Neural Information Processing Systems, 33:2051–2061, 2020.
- Jia Deng, Wei Dong, Richard Socher, Li-Jia Li, Kai Li, and Li Fei-Fei. Imagenet: A large-scale hierarchical image database. In 2009 IEEE conference on computer vision and pattern recognition, pages 248–255. Ieee, 2009.
- Prafulla Dhariwal and Alexander Nichol. Diffusion models beat gans on image synthesis. Advances in neural information processing systems, 34:8780–8794, 2021.
- Yinpeng Dong, Huanran Chen, Jiawei Chen, Zhengwei Fang, Xiao Yang, Yichi Zhang, Yu Tian, Hang Su, and Jun Zhu. How robust is google’s bard to adversarial image attacks? arXiv preprint arXiv:2309.11751, 2023.
- Executive Office of the President. Executive order 14110: Safe, secure, and trustworthy development and use of artificial intelligence. Federal Register, 88:75191–75226, 2023.
- Pierre Fernandez, Alexandre Sablayrolles, Teddy Furon, Hervé Jégou, and Matthijs Douze. Watermarking images in self-supervised latent spaces. In ICASSP 2022-2022 IEEE International Conference on Acoustics, Speech and Signal Processing (ICASSP), pages 3054–3058. IEEE, 2022.
- Pierre Fernandez, Guillaume Couairon, Hervé Jégou, Matthijs Douze, and Teddy Furon. The stable signature: Rooting watermarks in latent diffusion models. arXiv preprint arXiv:2303.15435, 2023.
- Jamie Hayes and George Danezis. Generating steganographic images via adversarial training. Advances in neural information processing systems, 30, 2017.
- Kaiming He, Xiangyu Zhang, Shaoqing Ren, and Jian Sun. Deep residual learning for image recognition. In Proceedings of the IEEE conference on computer vision and pattern recognition, pages 770–778, 2016.
- Martin Heusel, Hubert Ramsauer, Thomas Unterthiner, Bernhard Nessler, and Sepp Hochreiter. Gans trained by a two time-scale update rule converge to a local nash equilibrium. Advances in neural information processing systems, 30, 2017.
- Jonathan Ho, Ajay Jain, and Pieter Abbeel. Denoising diffusion probabilistic models. Advances in neural information processing systems, 33:6840–6851, 2020.
- Alain Hore and Djemel Ziou. Image quality metrics: Psnr vs. ssim. In 2010 20th international conference on pattern recognition, pages 2366–2369. IEEE, 2010.
- Andrew Ilyas, Shibani Santurkar, Dimitris Tsipras, Logan Engstrom, Brandon Tran, and Aleksander Madry. Adversarial examples are not bugs, they are features. Advances in neural information processing systems, 32, 2019.
- Nathan Inkawhich, Wei Wen, Hai Helen Li, and Yiran Chen. Feature space perturbations yield more transferable adversarial examples. In Proceedings of the IEEE/CVF Conference on Computer Vision and Pattern Recognition, pages 7066–7074, 2019.
- Hengrui Jia, Christopher A Choquette-Choo, Varun Chandrasekaran, and Nicolas Papernot. Entangled watermarks as a defense against model extraction. In 30th USENIX Security Symposium (USENIX Security 21), pages 1937–1954, 2021.

Zhengyuan Jiang, Jinghui Zhang, and Neil Zhenqiang Gong. Evading watermark based detection of ai-generated content. [arXiv preprint arXiv:2305.03807](#), 2023.

Diederik P Kingma and Max Welling. Auto-encoding variational bayes, 2022.

Tuomas Kynkäänniemi, Tero Karras, Samuli Laine, Jaakko Lehtinen, and Timo Aila. Improved precision and recall metric for assessing generative models. [Advances in Neural Information Processing Systems](#), 32, 2019.

Tuomas Kynkäänniemi, Tero Karras, Miika Aittala, Timo Aila, and Jaakko Lehtinen. The role of imagenet classes in fr\`echet inception distance. [arXiv preprint arXiv:2203.06026](#), 2022.

Tsung-Yi Lin, Michael Maire, Serge Belongie, James Hays, Pietro Perona, Deva Ramanan, Piotr Dollár, and C Lawrence Zitnick. Microsoft coco: Common objects in context. In [Computer Vision–ECCV 2014: 13th European Conference, Zurich, Switzerland, September 6–12, 2014, Proceedings, Part V 13](#), pages 740–755. Springer, 2014.

Nils Lukas and Florian Kerschbaum. Ptw: Pivotal tuning watermarking for pre-trained image generators. [arXiv preprint arXiv:2304.07361](#), 2023.

Nils Lukas, Abdulrahman Daa, Lucas Fenaux, and Florian Kerschbaum. Leveraging optimization for adaptive attacks on image watermarks. [arXiv preprint arXiv:2309.16952](#), 2023.

Aleksander Madry, Aleksandar Makelov, Ludwig Schmidt, Dimitris Tsipras, and Adrian Vladu. Towards deep learning models resistant to adversarial attacks. [arXiv preprint arXiv:1706.06083](#), 2017.

Weili Nie, Brandon Guo, Yujia Huang, Chaowei Xiao, Arash Vahdat, and Anima Anandkumar. Diffusion models for adversarial purification. [arXiv preprint arXiv:2205.07460](#), 2022.

JJK ó Ruanaidh, WJ Dowling, and FM Boland. Watermarking digital images for copyright protection. [IEE PROCEEDINGS VISION IMAGE AND SIGNAL PROCESSING](#), 143:250–256, 1996.

Joseph JK O’Ruanaidh and Thierry Pun. Rotation, scale and translation invariant digital image watermarking. In [Proceedings of International Conference on Image Processing](#), pages 536–539. IEEE, 1997.

Dustin Podell, Zion English, Kyle Lacey, Andreas Blattmann, Tim Dockhorn, Jonas Müller, Joe Penna, and Robin Rombach. Sdxl: Improving latent diffusion models for high-resolution image synthesis. [arXiv preprint arXiv:2307.01952](#), 2023.

Alec Radford, Jong Wook Kim, Chris Hallacy, Aditya Ramesh, Gabriel Goh, Sandhini Agarwal, Girish Sastry, Amanda Askell, Pamela Mishkin, Jack Clark, et al. Learning transferable visual models from natural language supervision. In [International conference on machine learning](#), pages 8748–8763. PMLR, 2021.

Robin Rombach, Andreas Blattmann, Dominik Lorenz, Patrick Esser, and Björn Ommer. High-resolution image synthesis with latent diffusion models. In [Proceedings of the IEEE/CVF conference on computer vision and pattern recognition](#), pages 10684–10695, 2022.

Bitar Darvish Rouhani, Huili Chen, and Farinaz Koushanfar. Deepsigns: A generic watermarking framework for ip protection of deep learning models. [arXiv preprint arXiv:1804.00750](#), 2018.

Mehrdad Saberi, Vinu Sankar Sadasivan, Keivan Rezaei, Aounon Kumar, Atoosa Chegini, Wenxiao Wang, and Soheil Feizi. Robustness of ai-image detectors: Fundamental limits and practical attacks. [arXiv preprint arXiv:2310.00076](#), 2023.

Jiaming Song, Chenlin Meng, and Stefano Ermon. Denoising diffusion implicit models. [arXiv preprint arXiv:2010.02502](#), 2020.

- Matthew Tancik, Ben Mildenhall, and Ren Ng. Stegastamp: Invisible hyperlinks in physical photographs. In Proceedings of the IEEE/CVF conference on computer vision and pattern recognition, pages 2117–2126, 2020.
- Zijie J Wang, Evan Montoya, David Munechika, Haoyang Yang, Benjamin Hoover, and Duen Horng Chau. Diffusiondb: A large-scale prompt gallery dataset for text-to-image generative models. arXiv preprint arXiv:2210.14896, 2022.
- Yuxin Wen, John Kirchenbauer, Jonas Geiping, and Tom Goldstein. Tree-ring watermarks: Fingerprints for diffusion images that are invisible and robust. arXiv preprint arXiv:2305.20030, 2023.
- Jiazheng Xu, Xiao Liu, Yuchen Wu, Yuxuan Tong, Qinkai Li, Ming Ding, Jie Tang, and Yuxiao Dong. Imagereward: Learning and evaluating human preferences for text-to-image generation. arXiv preprint arXiv:2304.05977, 2023.
- Ning Yu, Vladislav Skripniuk, Sahar Abdelnabi, and Mario Fritz. Artificial fingerprinting for generative models: Rooting deepfake attribution in training data. In Proceedings of the IEEE/CVF International conference on computer vision, pages 14448–14457, 2021.
- Yu Zeng, Mo Zhou, Yuan Xue, and Vishal M Patel. Securing deep generative models with universal adversarial signature. arXiv preprint arXiv:2305.16310, 2023.
- Kevin Alex Zhang, Lei Xu, Alfredo Cuesta-Infante, and Kalyan Veeramachaneni. Robust invisible video watermarking with attention. arXiv preprint arXiv:1909.01285, 2019.
- Richard Zhang, Phillip Isola, Alexei A Efros, Eli Shechtman, and Oliver Wang. The unreasonable effectiveness of deep features as a perceptual metric. In CVPR, 2018.
- Xuandong Zhao, Kexun Zhang, Zihao Su, Saastha Vasan, Ilya Grishchenko, Christopher Kruegel, Giovanni Vigna, Yu-Xiang Wang, and Lei Li. Invisible image watermarks are provably removable using generative ai, 2023a.
- Yunqing Zhao, Tianyu Pang, Chao Du, Xiao Yang, Ngai-Man Cheung, and Min Lin. A recipe for watermarking diffusion models. arXiv preprint arXiv:2303.10137, 2023b.
- Jiren Zhu, Russell Kaplan, Justin Johnson, and Li Fei-Fei. Hidden: Hiding data with deep networks. In Proceedings of the European conference on computer vision (ECCV), pages 657–672, 2018.

Benchmarking the Robustness of Image Watermarks

Supplementary Material

A Formalism of Watermark Detection and Identification

Invisible image watermarks, which are inspired by classical watermarks to protect the intellectual properties of creators, are now applied for a wider range of application scenarios. With the vast development of AI generative models, most current research focuses on applying invisible watermarks to (1) identify AI-generated images (AI Detection) (Saber et al., 2023), and (2) identify the user who generated the image for source tracking (User Identification) (Fernandez et al., 2023).

To fairly evaluate the different watermark methods for different applications, we start from formulating a general, message-based watermarking protocol, partially adopting the notation of (Lukas et al., 2023), which generalizes most of the existing setups. Let θ_G denote an image generator, \mathcal{M} the space of watermark messages, and \mathcal{X} the domain of images. We assume \mathcal{M} is a metric space with distance function $D(\cdot, \cdot)$. The choice of message space \mathcal{M} can be very different depending on the watermarking algorithm: for Tree-Ring, messages are random complex Gaussians, while for the Stable Signature and StegaStamp, each message is a length- d binary string, where d denotes the length of the message. For watermarking algorithms following the encoder-decoder training approach, like Stable Signature and StegaStamp, the choice of message length d is fixed after training. Some methods, such as Tree-Ring, enjoy flexible message length at the time of injecting watermarks.

In addition to classifying images as watermarked or non-watermarked, a good detector will often provide a p -value for the watermark detection, which measures the probability that the level of watermark strength observed in an image could occur by random chance. The Tree-Ring watermark also includes an image location parameter τ to embed a message $m \in \mathcal{M}$, but we subsume this under the parameters of θ_G . We now introduce several important watermarking operations:

- **EMBED**: $\theta_G \times \mathcal{M} \rightarrow \mathcal{X}$ is the generative procedure that creates a watermarked image given user-defined parameters of θ_G (such as prompt, guidance scale, etc. for a diffusion model) and a target message $m \in \mathcal{M}$.
- **DECODE**: $\mathcal{X} \rightarrow \mathcal{M}$ is a recovery procedure of a message m embedded within a watermarked image $x = \text{EMBED}(\theta_G, m)$. In particular, the recovery $m' = \text{DECODE}(x)$ may be imperfect, i.e., $m' \neq m$.
- **VERIFY** $_\alpha$: $\mathcal{M} \times \mathcal{M} \rightarrow \{0,1\}$ is conducted by the model owner to decide whether x was watermarked by inspecting $m' = \text{DECODE}(x)$, where $x = \text{EMBED}(\theta_G, m)$. For a decoded message m' , we consider the following p -value (further discussed in Section B) for evaluating whether the image could have been watermarked using m . which is defined as

$$p = \mathbb{P}_m(D(\omega, m') < D(m, m') | H_0),$$

where, $D(\omega, m')$ is the similarity between an arbitrary message $\omega \sim \mathcal{M}$ (drawn uniformly at random) and m' , and $D(m, m')$ is the similarity between the ground truth message m and the recovered message m' . H_0 denotes the null hypothesis that the image was generated without knowledge of the watermark (and therefore the recovered message is random). **VERIFY** $_\alpha(m', m)$ returns 1 if $p < \alpha$, and 0 otherwise. In our experiments, we set $\alpha = 0.001$.

To establish a comprehensive evaluation toolbox, we consider two distinct problems that naturally arise during watermark analysis: detection and identification. Let $\mathcal{A}: \mathcal{X} \rightarrow \mathcal{X}$ represent an image attack function and denote by Q a fixed subset of messages independently drawn from \mathcal{M} used by θ_G . Further, assume that the owner of θ_G will only embed messages contained within a finite subset Q drawn randomly from \mathcal{M} .

A.1 Detection

In the *watermark detection problem*, given $x = \text{EMBED}(\theta_G, m)$, and an attack $x' = \mathcal{A}(x)$, the model owner is tasked with producing EMBED and DECODE protocols which satisfy the following,

- (1) If $x = \text{EMBED}(\theta_G, m)$ is a watermarked image, then $\text{VERIFY}_\alpha(\text{DECODE}(x')) = 1$.
- (2) If $x = \text{EMBED}(\theta_G, \text{NULL})$ is an unwatermarked image, then $\text{VERIFY}_\alpha(\text{DECODE}(x')) = 0$.

For both conditions, a comparison of the extracted message $m' = \text{DECODE}(x)$ is performed against all messages in Q . Failure of the above conditions is referred to as Type II and Type I errors, respectively. Exploration of the tradeoff between minimization of both error types is an interesting research topic in its own right (Saberi et al., 2023, Zhao et al., 2023a).

A.2 Identification

While watermark detection requires only that $\text{VERIFY}(\theta_G, x') = 1$, the *watermark identification problem* further requires that one can accurately determine which message from Q is embedded in the image. Rigorously, given $x = \text{EMBED}(\theta_G, m)$, an attack $x' = \mathcal{A}(x)$, and $m' = \text{DECODE}(\theta_G, x')$, the user requires the EMBED and DECODE to satisfy

$$\underset{m' \in Q}{\text{argmin}} \ P(D(\omega, m) < D(m', m) \mid H_0) = m,$$

for randomly drawn $\omega \sim \mathcal{M}$ if x .

The identification problem is useful in the scenario where the model owner wishes to identify the user who created an image (e.g., a user of DALL·E). Note that as $|Q| \rightarrow \infty$, the identification problem becomes difficult as Q will resemble \mathcal{M} in distribution.

B Details on Performance Metrics

B.1 Clarifications on p -Value

Here, we clarify the definition of the p -value as follows.

Watermark injection and evaluation are often done by encoding a message m into the image, and later recovering the message m' , which may be an imperfect recovery. In addition to classifying images as watermarked or non-watermarked, a good detector will often provide a p -value for the watermark detection, which measures the probability that the level of watermark strength observed in an image could happen by random chance. Rigorously, we have

$$p = P_m(D(\omega, m') < D(m, m') \mid H_0),$$

where $D(\omega, m')$ is a dissimilarity metric between an arbitrary message $\omega \sim \mathcal{M}$ (selected uniformly at random) and recovered message m' from the image by the detector, and $D(m, m')$ denotes dissimilarity between the ground truth message m and the recovered message m' . H_0 denotes the null hypothesis that the image was generated without knowledge of the watermark (and therefore, the recovered message is random). The same hypothesis testing can also be applied to user identification.

As in some prior work (Fernandez et al., 2023), one may set a threshold on the estimated p -value to determine the detection result. However, this approach makes it difficult to compare different watermark methods fairly. Even if we set the same p -value threshold on all watermark methods, the distinct choice of message space \mathcal{M} ,

message distribution P_m , and hypothesis test may differ. Therefore, we seek to evaluate watermark methods mainly using metrics that are independent of the choice of p -value threshold and statistical test.

B.2 Performance Metrics for User Identification

For user identification, we also focus on metrics that do not depend on statistical testing and hyperparameters like p -value thresholds.

The user detection issue involving K users is aptly conceptualized as a K -way classification task. This can be reframed into a binary classification problem by designating the positive class as the correct user and the negative class as all other users. From this perspective, the $\text{TPR}@x\%\text{FPR}$ metric becomes applicable, defined for a specific FPR threshold and user count. In our study, we focus on $\text{TPR}@0.1\%\text{FPR}$ for a scenario involving 1,000 users. The identification performance results are shown in Section 4.4.

B.3 Other Performance Metrics

While this paper primarily focuses on the $\text{TPR}@0.1\%\text{FPR}$ metric, it's important to acknowledge other common metrics such as p -values, AUROC scores, mean accuracies, and bit accuracies.

However, we do not report p -values since their absolute values depend heavily on the chosen statistical test, making them less comparable across different watermark methods.

AUROC scores, although independent of the choice of p -value threshold and statistical test, have limitations used as a metric for evaluating watermark detection. In AI-generated image applications, labeling non-watermarked images as watermarked (false positive) are particularly detrimental. As a result, strict control of false positive rate (FPR) is crucial. However, a high AUROC does not guarantee a high true positive rate (TPR) at low false positive rate (FPR) levels.

Using message distances such as bit accuracy as a metric for evaluating watermarks' performance has several limitations:

- (1) Insensitivity to error distribution: bit accuracy measures the proportion of correctly identified bits in the watermark but does not account for the distribution of errors. This means it treats all errors equally, regardless of their impact or pattern. In watermarking, certain types of errors (like clustered errors) might be more detrimental than others.
- (2) Lack of contextual insight: bit accuracy alone doesn't provide insights into the types of errors (false positives or false negatives). In watermark detection, understanding the nature of errors is crucial, especially in differentiating between missing a watermark and incorrectly identifying one.
- (3) Threshold dependency: the effectiveness of bit accuracy is dependent on the threshold chosen for determining a bit's value. Different thresholds can yield significantly different bit accuracies, making the metric somewhat arbitrary and less reliable for comparing different watermarking schemes.
- (4) Non-representation of overall system performance: bit accuracy focuses narrowly on the correctness of individual bits, neglecting the broader context of the watermarking system's performance, such as its robustness against attacks, computational efficiency, or impact on image quality.
- (5) Potential misleading results in imbalanced cases: in scenarios where the watermark bits are not evenly distributed (e.g., more 0s than 1s or vice versa), bit accuracy might give a skewed view of the system's performance. It could show high accuracy even if the system is only good at detecting the majority class. For these reasons, it's often more effective to use a combination of metrics that can provide a holistic view of the watermarking system's performance, considering aspects like error distribution, false positives/negatives, and overall impact on the media.

Although these metrics are not included in the paper, they are incorporated in the benchmark software and available for future research use.

C Design Choices of WAVES

C.1 Dataset Preparation

In this paper, we consider three different datasets, DiffusionDB, MS-COCO, and DALL·E3, each consisting of 5,000 pairs of reference images and prompt strings. The three datasets are filtered subsets of the corresponding source dataset using the same filtering algorithm. The source dataset information is listed below.

- *DiffusionDB*: the 2m_random_100k split of DiffusionDB dataset (Wang et al., 2022), [link](#).
- *MS-COCO*: the validation split of the 2017 Microsoft COCO detection challenge (Lin et al., 2014), [link](#).
- *DALL·E3*: the train split of the *dalle-3-dataset* repository on HuggingFace, collected from the LAION share-dalle-3 discord channel, [link](#).

The filtering algorithm considers the following rules to subsample the 5,000 image subset:

- *Remove columns*: Remove irrelevant columns and only keep the reference images and prompt strings.
- *Filter prompts*: Tokenize the prompt strings by the Open Clip’s tokenizer, and filter out samples with no tokens and more than 75 tokens. This is because Stable Diffusion (Rombach et al., 2022) truncates prompts at 75 tokens (Wang et al., 2022).
- *Rank images*: Rank the images by their aesthetics score, as defined by (Xu et al., 2023), in descending order. We then select the top 5,000 images, along with their corresponding prompt strings. This approach is adopted because the DiffusionDB and DALL·E3 datasets, sourced from chat-bots, contain some lower-quality images. We posit that watermarking holds greater utility for high-quality AI-generated images, as the copyright protection of low-quality generated images is less meaningful and practical.

In our study, we examined three distinct datasets—DiffusionDB, MS-COCO, and DALL·E3—each characterized by a unique distribution of prompt words. As illustrated in the word-cloud plots (Figure 15), we observe notable differences. DiffusionDB predominantly features prompt words that emphasize the desired quality of the generated images, such as “beautiful” and “highly detailed.” In contrast, MS-COCO’s prompts mainly focus on describing the objects within the images. Meanwhile, DALL·E3’s prompts show a tendency towards describing aspects of fine arts.



Figure 15. Word clouds of DiffusionDB, MS-COCO, and DALL·E3 prompts.

Image examples from the three datasets are illustrated in Figure 16. The reference images for DiffusionDB are produced by Stable Diffusion, MS-COCO includes real-world photographs, and DALL·E3 contains images generated by the DALL·E3 model. This choice of datasets effectively covers two popular generative models and the real-world scenario, highlighting their relevance in practical watermarking applications.



Figure 16. Image examples of DiffusionDB, MS-COCO, and DALL·E3.

C.2 Selection of Watermark Representatives

Table 4. A list of alternative watermarking algorithms not tested by WAVES in this work.

Method	Known Weakness(es)
DwtDet (Al-Haj, 2007)	Distortion (Wen et al., 2023), Purification (Saber et al., 2023)
DwtDetSvd (Al-Haj, 2007)	Distortion (Wen et al., 2023, Zhao et al., 2023a), Purification (Saber et al., 2023), Regeneration (Zhao et al., 2023a)
RivaGan (Dong et al., 2023)	Regeneration (Zhao et al., 2023a), Purification (Saber et al., 2023)
SSL (Fernandez et al., 2022)	Distortion (Zhao et al., 2023a), Regeneration (Zhao et al., 2023a)
WatermarkDM (Zhao et al., 2023b)	Purification (Saber et al., 2023)

Our WAVES framework can be used to stress-test the robustness of any watermark. In this work, however, we focus on three methods: the *Stable Signature*, *Tree-Ring*, and *Stegastamp*. This is due to existing and extensive studies (Saber et al., 2023, Wen et al., 2023, Zhao et al., 2023a) indicating these three methods are far more robust to simple off-the-shelf attacks than alternative watermarking algorithms listed in Section 2.1. We list these competitors along with their documented vulnerabilities in Table 4.

D Evaluation Details

In this section, we provide more details on the evaluation scheme of WAVES.

D.1 Details on Identification Setups

We treat the user identification problem as a multi-class classification task, as outlined in Section 3.1. This involves defining a set of ground-truth messages, each corresponding to a unique user. To avoid the exhaustive evaluation process (watermark encoding, attacking, and decoding) for varying numbers of users, we consistently watermark images with the same message, the ground-truth message of the first user, and generate a random set of ground-truth messages for the remaining users at the time of evaluation. This approach is feasible since the ground-truth messages for users other than the first do not influence the watermarking or attack phases. We conduct the identification assessment ten times with ten distinct random sets of ground-truth messages for the other users, and we report the mean multi-class classification accuracy.

D.2 Normalization and Aggregation of Quality Metrics

In Figure 17, the cumulative distribution functions (CDFs) for eight image quality metrics over all attacked watermarked images are presented. This illustration includes the metric values at the 10% and 90% quantiles, which are used as the boundaries for normalizing the metric values within the range of $[0.1, 0.9]$. Such normalization ensures that all normalized metrics exhibit a comparable statistical distribution over attacked watermarked images, facilitating an unbiased aggregated evaluation. To consolidate these normalized metrics, we first calculate the average within each of the four defined categories (image similarities, distribution distances, perception-based metrics, and image quality assessments) as delineated in Section 3.1.3. Subsequently, the average of these category averages is calculated to yield a single, consolidated normalized, and aggregated quality metric.

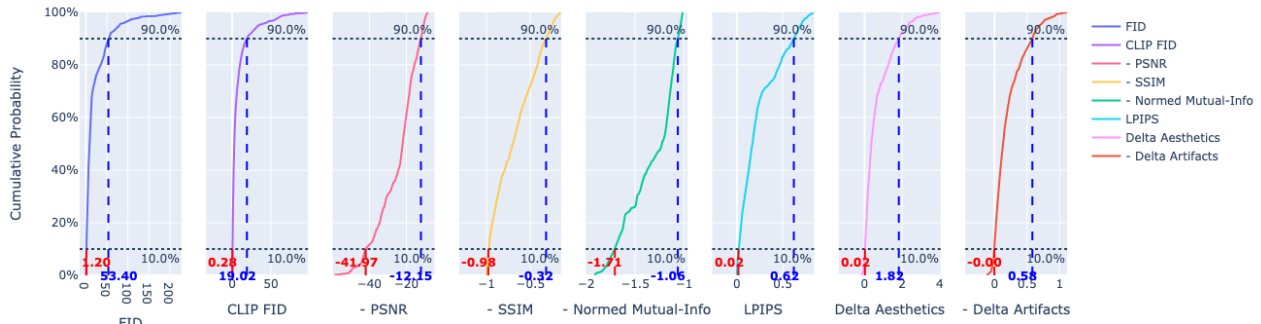


Figure 17. Cumulative distribution functions (CDFs) for eight image quality metrics across all attacked watermarked images. The horizontal dashed lines mark the 10% and 90% quantiles, and the intersecting vertical dashed lines delineate the bounds of the normalization intervals. Values at the lower bound are normalized to 0.1, and those at the upper bound to 0.9.

D.3 Attacks Considered for Benchmarking Watermarks

When benchmarking watermark robustness in Figure 12 and Figure 14, we consider the following effective attacks. We select 21 attacks from 26 attacks. We include all distortion attacks. We select the two most effective single regeneration attacks and two rinsing attacks. For adversarial attacks, we do not include AdvEmbB-RN18, and AdvCls-Real&WM since they basically do not work. We also eliminate AdvCls-UnWM&WM and only use AdvCls-WM1&WM2 to represent surrogate detector attacks since AdvCls-UnWM&WM is based on an unrealistic assumption.

- *Distortion Single*: Dist-Rotation, Dist-RCrop, Dist-Erase, Dist-Bright, Dist-Contrast, Dist-Blur, Dist-Noise, Dist-JPEG.
- *Distortions Combination*: DistCom-Geo, DistCom-Photo, DistCom-Deg, DistCom-All.
- *Regeneration Single*: Regen-Diff, Regen-KLVAE.
- *Regeneration Rinsing*: Regen-2xDiff, Regen-4xDiff.
- *Adv Embedding Grey-box*: AdvEmbG-KLVAE8.
- *Adv Embedding Black-box*: AdvEmbB-CLIP, AdvEmbB-SdxlVAE, AdvEmbB-KLVAE16.
- *Adv Surrogate Detector*: AdvCls-WM1&WM2.

E Details of Attacks

E.1 Distortion Attacks

For single distortions, we consider, as described in Section 3.2, eight types: rotation, resized-crop, random erasing, brightness adjustment, contrast adjustment, Gaussian blur, Gaussian noise, and JPEG compression. For each distortion, we consider five evenly distributed distortion strengths between minimum and maximum; the minimums and maximums are listed as follows.

- *Rotation*: rotate 9° to 45° clock-wise.
- *Resized-crop*: crop 10% to 50% of the image area.
- *Random erasing*: erase 5% to 25% of the image area and fill with gray color.
- *Brightness adjustment*: increase image brightness by 20% to 100%.
- *Contrast adjustment*: increase image contrast by 20% to 100%.

- *Gaussian blur*: blur with kernel size from 4 to 20 pixels.
- *Gaussian noise*: add Gaussian random noise with standard deviation from 0.02 to 0.1 (when pixel values normalized to $[0, 1]$).
- *JPEG compression*: compress with JPEG quality score from 90 to 10.

It is worth noting that our strength selections are more conservative than most of the watermark papers, such as (Fernandez et al., 2023, Wen et al., 2023). This is because we want to keep the image quality after distortion within a reasonable interval compared to the other attacks. While some watermark papers intentionally select unreasonably large distortion strength (for example, cropping 90% of image area in (Fernandez et al., 2023), or Gaussian blurring with kernel size 40 (Wen et al., 2023)) to demonstrate their robustness under some distortions. We implement the distortions following the standard image augmentations in the *torchvision* library.

For combinations of distortions (also called combo distortions in paper for short), we apply each single distortion with the same relative strength, where the relative strength is between 0 and 1, normalized with respect to the minimum and maximum strengths above. For combinations of geometric, photometric, and degradation distortions, we consider five evenly distributed normalized strengths from 0.05 to 0.45. For combinations of all distortions, we consider five evenly distributed normalized strengths from 0.05 to 0.20. The relative strengths are selected for reasonable image qualities after distortions again.

E.2 Regeneration Attacks

Following the language of Section 3, regeneration attacks (Zhao et al., 2023a) use off-the-shelf VAEs and diffusion models to transfer a target image $x \in \mathcal{X}$ to a latent representation followed by a restoration to $x' \in \mathcal{X}$ that is faithful to its original representation, i.e., $x' \approx x$. Since the chosen VAE or diffusion model will not be contained by the attacker’s model of interest, the entire regeneration is likely to disrupt the latent representation of x , thereby damaging an embedded watermark. However, since the capacity of the attacker’s regenerative model is inferior to the target model, x' will likely be of reduced quality. In this work, the target model is Stable Diffusion v2.1 while the surrogate model used for regeneration is Stable Diffusion v1.4.

Figure 6 demonstrates that a long diffusion or low-quality VAE attack will significantly reduce watermark detectability but at the expense of reduced image quality, which is clear by visual inspection of the sequence of images in Figure 18. Rising regenerations achieve similar reductions in detection, although too deep of rinsing regenerations (> 30 noising steps) significantly alter image quality as evidenced by Figure 19.

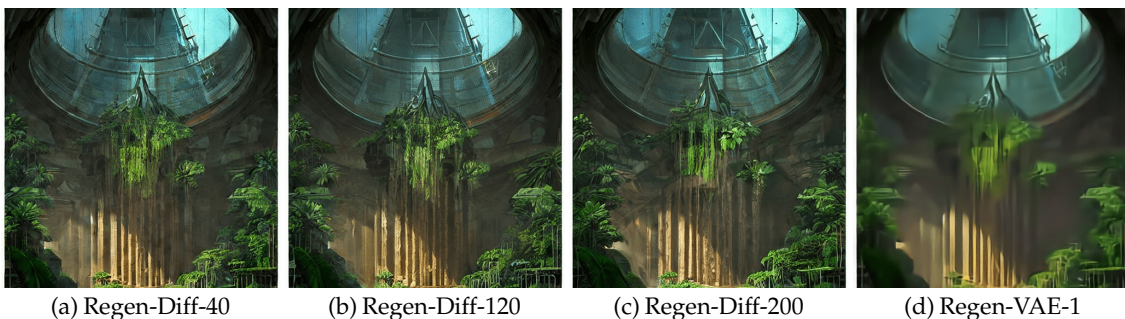


Figure 18. Regenerative diffusion with varying depth of noising steps and a VAE regeneration with a low quality factor.



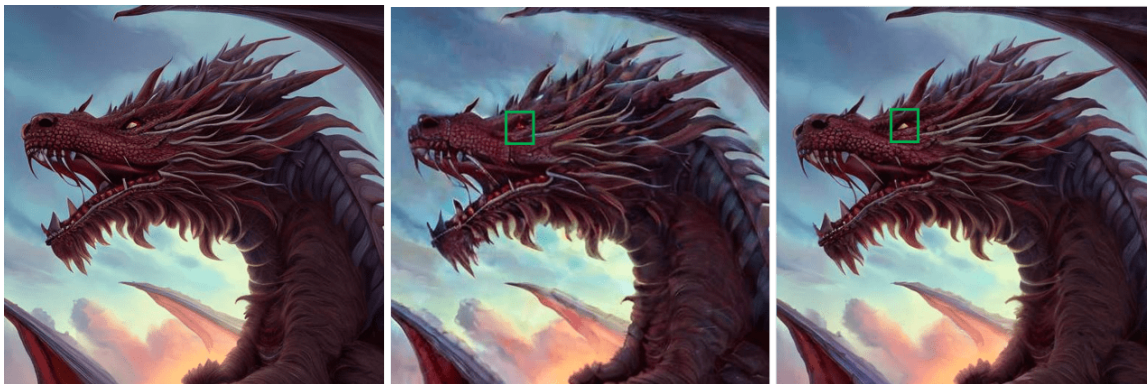
(a) Rinse-4xDiff-10 (b) Regen-4xDiff-30 (c) Regen-4xDiff-50
 Figure 19. 4x rinsing regeneration with varying depth of noising steps per diffusion.

E.2.1 Prompted Regeneration

This work proposes a simple variation on a regenerative diffusion attack: if an image is produced via a known prompt, then an attacker uses the prompt to guide the diffusion of their surrogate model. This type of attack is reasonable and realistic for users of online generative models such as DALL-E or Midjourney. Figure 6 and Tables 5 & 3 indicate that this type of attack, labeled Regen-DiffP is slightly stronger than conventional Regen-Diff.

E.2.2 Mixed Regeneration

Mixed regeneration refers to any style of attack that uses a regenerative diffusion on an image followed by VAE-style regeneration for the purposes of denoising. In Figure 6, we label examples of such attacks as RinseD-VAE and RegenD-KLVAE, which respectively denote VAE and KLVAE denoising following a 4x rinsing regeneration with 50 steps (Rinse-4xDiff-50). According to Figure 6, such a combination improves PSNR and CLIP-FID, as opposed to a Rinse-4xDiff alone. The restorative effects of mixed regeneration are visually observable for shallower (i.e., 2x or 3x) rinsing regenerations, as depicted in Figure 20. We do not extensively study or rank such attacks in this work, but include them as a future topic of research.



(a) Unattacked (b) Rinse-3xDiff (c) Rinse-3xDiff+VAE

Figure 20. An image of a dragon attacked using a 3x rinsing regeneration. Pushing the image through a VAE restores image quality, noticeable in the eye color of the dragon (indicated by the green box). Image is drawn from the Gustavosta Stable Diffusion dataset available @ <https://huggingface.co/datasets/Gustavosta/Stable-Diffusion-Prompts>.

All tested regeneration attacks are summarized as follows, with five evenly divided strengths between the listed minimum and maximum unless specified otherwise:

- *Regeneration via diffusion*: passes an image through Stable Diffusion v1.4 with strength as the number of noise/ de-noising steps timesteps, 40 to 200.
- *Regeneration via prompted diffusion*: passes an image through Stable Diffusion v1.4 conditioned on its generative prompt with strength as the number of noise/ de-noising steps timesteps, 40 to 200.
- *Regeneration via VAE*: Image is encoded then decoded by a pre-trained VAE (Ballé et al., 2018) with strength as quality level from 1 to 7.
- *Regeneration via KL-VAE*: Image is encoded and then decoded by a pre-trained KL-regularized autoencoder with strength as bottleneck sizes 4, 8, 16, or 32.
- *Rinsing generation 2x*: an image is noised then de-noised by Stable Diffusion v1.4 two times with strength as number of timesteps, 20-100 (per diffusion).
- *Rinsing generation 4x*: an image is noised then de-noised by Stable Diffusion v1.4 two times with strength as number of timesteps, 10-50 (per diffusion).
- *Mixed Regeneration via VAE*: an image passed through a rinsing regeneration 4x (for 50 timesteps each) and then a VAE with strength as quality level from 1-7.
- *Mixed Regeneration via KL-VAE*: an image passed through a rinsing regeneration 4x (for 50 timesteps each) and then a KL-VAE with strength as bottleneck sizes 4, 8, 16, or 32.

E.3 Adversarial Attacks

E.3.1 Embedding Attack

The embedding attacks use off-the-shelf encoders and perform untargeted attacks. We use the Projected Gradient Descent (PGD) algorithm (Madry et al., 2017) to optimize the adversarial examples. We conduct the attack using a range of perturbation budgets ϵ , specifically {2/255, 4/255, 6/255, 8/255}. All the attacks are configured with a step size of $\alpha = 0.05 * \epsilon$ and the number of total iterations of 200. The attacks are on the watermarked images, aiming to remove the watermarks by perturbing their latent representations.

E.3.2 Surrogate Detector Attack

Figure 8 illustrates the three settings of training the surrogate detectors. In all three settings, we train the surrogate detectors by fine-tuning the ResNet18³ for 10 epochs with a learning rate of 0.001 and a batch size of 128. The training images are either generated by the victim generator with the ImageNet text prompts "A photo of a {ImageNet class name}," or real ImageNet images. We randomly shuffle those images and build the binary training set according to each setting. In the AdvCls-UnWM&WM setting, we train the surrogate detector with 3000 images (1500 images per class) since we find a larger training set might have the overfitting problem. In the AdvCls-Real&WM and AdvCls-WM1&WM2 settings, we train the surrogate detector with 15000 images (7500 images per class). The watermarked images in AdvCls-WM1&WM2 are embedded with two distinct messages. One message is the one used in the test watermarked images. The other one is randomly generated. In all three settings, we use 5000 images (2500 images per class) for validation (derived from the same source as the training set), and the training yields nearly 100% validation accuracy in all cases.

After completing the training phase, the adversary executes a Projected Gradient Descent (PGD) attack on the surrogate detector using the testing data (DiffusionDB, MS-COCO, DALL·E3). In all three settings, we conduct the attack using a range of perturbation budgets ϵ , specifically {2/255, 4/255, 6/255, 8/255}. The attack is configured with a step size of $\alpha = 0.01 * \epsilon$ and the number of total iterations of 50. By flipping the label, the adversary can either try to remove the watermarks or add the watermarks. The analyses of results appear in Appendix F.2.

³<https://pytorch.org/vision/main/models/generated/torchvision.models.resnet18.html>

F Additional Results

F.1 More Results for Identification

Table 5 presents the ranking of attacks in the identification setup.

Table 5. **Comparison of attacks across three watermarking methods under the identification setup (one million users).** Q denotes the normalized quality degradation and P denotes the performance as derived from aggregated 2D plots. Q@0.7P measures quality degradation at a 0.7 performance threshold where "inf" denotes cases where all tested attack strengths yield performance above 0.7, and "-inf" where all are below. Q@0.4P is defined analogously. Avg P and Avg Q are the average performance and quality over all the attack strengths. The lower the performance and the smaller the quality degradation, the stronger the attack. For each watermarking method, we rank attacks by Q@0.7P, Q@0.4P, Avg P, Avg Q, in that order, with lower values (↓) indicating stronger attacks. The top 5 attack of each watermarking method are highlighted in red.

Attack	Tree-Ring					Stable Signature					StegaStamp				
	Rank	Q@0.7P	Q@0.4P	Avg P	Avg Q	Rank	Q@0.7P	Q@0.4P	Avg P	Avg Q	Rank	Q@0.7P	Q@0.4P	Avg P	Avg Q
Dist-Rotation	8	-inf	0.434	0.131	0.648	12	0.613	0.642	0.400	0.650	4	0.454	0.500	0.288	0.616
Dist-RCrop	11	-inf	0.592	0.094	0.463	24	inf	inf	0.972	0.461	6	0.602	0.602	0.494	0.451
Dist-Erase	26	inf	inf	0.986	0.490	25	inf	inf	0.988	0.489	25	inf	inf	1.000	0.483
Dist-Bright	22	inf	inf	0.913	0.304	23	inf	inf	0.982	0.305	22	inf	inf	0.995	0.317
Dist-Contrast	23	inf	inf	0.949	0.243	20	inf	inf	0.979	0.243	17	inf	inf	0.994	0.231
Dist-Blur	21	1.105	1.437	0.551	1.221	5	-inf	-inf	0.000	1.204	9	0.897	0.970	0.280	1.198
Dist-Noise	16	0.427	inf	0.728	0.395	8	0.415	0.480	0.633	0.390	24	inf	inf	1.000	0.360
Dist-JPEG	17	0.499	0.499	0.700	0.284	9	0.485	0.485	0.540	0.284	21	inf	inf	0.995	0.263
DistCom-Geo	9	-inf	0.559	0.105	0.768	13	0.788	0.835	0.519	0.767	7	0.676	0.717	0.359	0.733
DistCom-Photo	23	inf	inf	0.947	0.242	20	inf	inf	0.981	0.243	17	inf	inf	0.994	0.239
DistCom-Deg	18	0.556	0.864	0.570	0.694	7	0.216	0.281	0.183	0.679	8	0.870	0.957	0.737	0.664
DistCom-All	10	-inf	0.575	0.123	0.908	11	0.550	0.623	0.176	0.900	10	0.995	1.096	0.682	0.870
Regen-Diff	6	-inf	0.307	0.258	0.323	1	-inf	-inf	0.000	0.300	2	0.333	inf	0.766	0.327
Regen-DiffP	6	-inf	0.308	0.256	0.327	1	-inf	-inf	0.000	0.303	1	0.336	0.356	0.763	0.329
Regen-VAE	19	0.578	0.578	0.701	0.348	10	0.545	0.545	0.340	0.339	23	inf	inf	1.000	0.343
Regen-KLVAE	14	0.257	inf	0.810	0.233	6	-inf	-inf	0.047	0.206	17	inf	inf	0.999	0.240
Rinse-2xDiff	5	-inf	0.270	0.220	0.357	3	-inf	-inf	0.000	0.332	3	0.390	0.402	0.778	0.366
Rinse-4xDiff	1	-inf	-inf	0.110	0.466	4	-inf	-inf	0.000	0.438	5	0.488	0.676	0.687	0.477
AdvEmbG-KLVAE8	4	-inf	0.168	0.259	0.253	20	inf	inf	0.985	0.249	17	inf	inf	1.000	0.232
AdvEmbB-RN18	15	0.288	inf	0.811	0.218	17	inf	inf	0.990	0.212	14	inf	inf	1.000	0.196
AdvEmbB-CLIP	20	0.697	inf	0.798	0.549	26	inf	inf	0.991	0.541	25	inf	inf	1.000	0.488
AdvEmbB-KLVAE16	12	0.158	0.309	0.540	0.238	19	inf	inf	0.983	0.233	14	inf	inf	1.000	0.206
AdvEmbB-SdxIVAE	13	0.214	inf	0.692	0.221	17	inf	inf	0.986	0.219	14	inf	inf	1.000	0.204
AdvCls-UnWM&WM	2	-inf	0.123	0.352	0.145	14	inf	inf	0.991	0.101	11	inf	inf	1.000	0.101
AdvCls-Real&WM	25	inf	inf	0.986	0.047	14	inf	inf	0.990	0.092	11	inf	inf	1.000	0.106
AdvCls-WM1&WM2	2	-inf	0.118	0.343	0.139	14	inf	inf	0.991	0.084	13	inf	inf	1.000	0.129

F.2 More Analyses on Surrogate Detector Attacks

The AdvCls-UnWM&WM attack leverages a surrogate model to distinguish between images that are watermarked and those that are not. As demonstrated in Figure 9, the PGD attack is effective in removing watermarks by flipping the label of watermarked images. This raises a question: Is it possible to similarly ‘add’ watermarks to clean images by flipping their labels? This process, commonly referred to as a spoofing attack, which demonstrates a false detection of watermarks in clean images, is explored in our study.

However, as illustrated in Figure 21, our attempts to add watermarks to clean images by simply flipping the labels were unsuccessful. In this experiment, detailed in Figure 21, we focus exclusively on unwatermarked images, aiming to introduce watermarks, while leaving already watermarked images untouched. Despite employing the most intensive perturbations, we were unable to artificially add

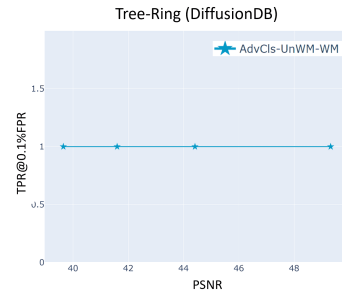


Figure 21. The spoofing attack fails for AdvCls-UnWM&WM.

watermarks to these images. This outcome leads to an intriguing inquiry: Why is the technique effective in removing watermarks but not in adding them? We delve into the underlying reasons for this asymmetry in Figure 22.

The insights from Figure 22 reveal that the surrogate model does not exactly remove the watermark. Instead, it perturbs the watermark along with other features within the latent space. The disturbance alone is sufficient to confuse the detector, making it challenging to recognize the watermark. In contrast, successfully adding watermarks requires precise modifications in the latent space, rather than mere perturbations, which proves to be a more challenging task. The relative imprecision of this attack may stem from the ‘transferable gap’ between the surrogate model and the ground-truth detector. Notably, for the purpose of watermark removal, perturbing the latent space proves to be adequately effective.

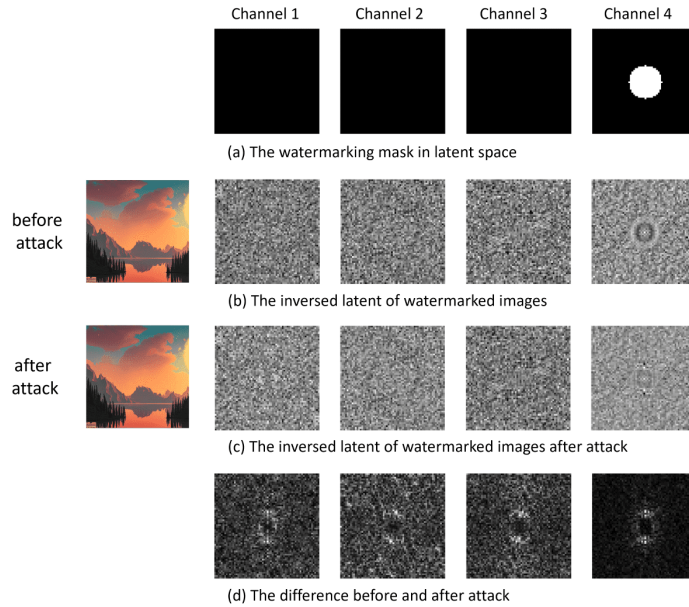


Figure 22. Visualization of AdvCls-UnWM&WM attack. (a) shows the watermarking mask of Tree-Ring where there are four channels, and we only watermark the last channel. The watermark message is the rings, which contain ten complex numbers that are not shown in the figure. (b) and (c) show the inversed latent before and after the attack in the Fourier space. We only show the real part of the latent. Clearly, the rings exist before the attack and vanish after the attack. (d) shows the magnitude of the element-wise difference before and after the attack. The attack not only perturbs the watermark part but also other features. The average magnitude change of the watermark-part and non-watermark-part is around 2:1. The attack successfully disturbs the watermark, albeit in an imprecise manner.

These findings have led to the development of our proposed AdvCls-WM1&WM2 attack, which utilizes images watermarked with different messages (e.g., collected from two users, User1 and User2). The essential requirement for this approach is the surrogate model’s ability to map images to the generator’s latent space. This mapping allows the attacker to perturb the latent space, removing the watermark. In contrast to the AdvCls-UnWM&WM approach, which uses both watermarked and non-watermarked images for training (differing only in the latent space), AdvCls-WM1&WM2 uses two sets of images, each embedded with a distinct watermark message (differing only in the latent space as well). Figure 23 shows that AdvCls-WM1&WM2 attack effectively disrupts the latent features of the images, including the watermarks. However, it lacks the precision to interchange the embedded watermark message. Consequently, while this attack can remove watermarks and mislead user identification—mistaking an image originally generated by User1 as belonging to another user—it cannot accurately manipulate the identification to frame User2 as desired by the attacker. The identification results in Figure 24 also support this finding. Although AdvCls-WM1&WM2 aims to misidentify images as belonging to User2, it often leads to misidentification as users other than User2. However, in a system with fewer users, like 100 users, and under intense attack conditions (e.g., strength=8), AdvCls-WM1&WM2 demonstrates

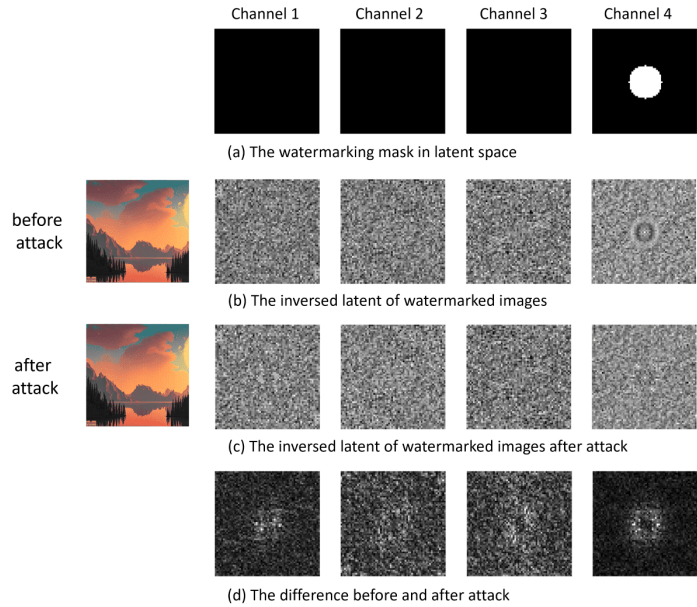


Figure 23. Visualization of AdvCls-WM1&WM2 attack. (a) and (b) are the same as that in Figure 22. (c) shows the inversed latent after the attack, where the watermark vanishes instead of changing to another watermark. (d) shows the magnitude of the element-wise difference before and after the attack. The attack not only perturbs the watermark part but also other features. The average magnitude change of the watermark-part and non-watermark-part is also around 2:1. Although the surrogate detector is trained to classify two different watermark messages. The attack based on it cannot change the watermark message from one to another but can effectively disturb the watermark.

a targeted identification success rate of 0.7%, showing a potential direction for attacks aimed at targeted user identification.

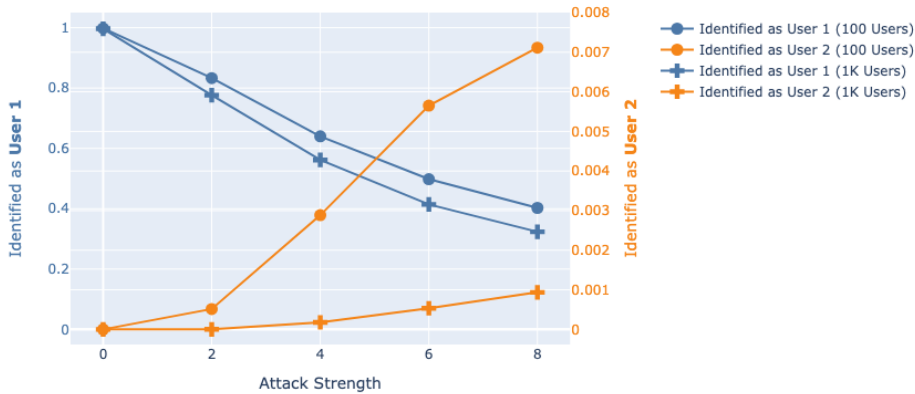


Figure 24. The user identification results for Tree-Ring under AdvCls-WM1&WM2 attacks. The original watermarked images are embedded with User1’s message. AdvCls-WM1&WM2 tries to disrupt the latent feature of those images so that they can be misidentified as User2 generated. We simulate two settings: 100 users and 1000 users in total. The blue curves represent the proportion of images correctly identified as belonging to User1, while the orange curves show those misidentified as User2’s. Note that, the axes for blue and orange curves have different ranges in the figure. With increasing attack strengths, the likelihood of correctly identifying them as User1’s decreases significantly under both 100 and 1K user scenarios. However, misidentification as User2’s images occurs notably only when the total number of users is small (e.g., 100 users).

F.3 Full Results on DiffusionDB, MS-COCO and DALL·E3

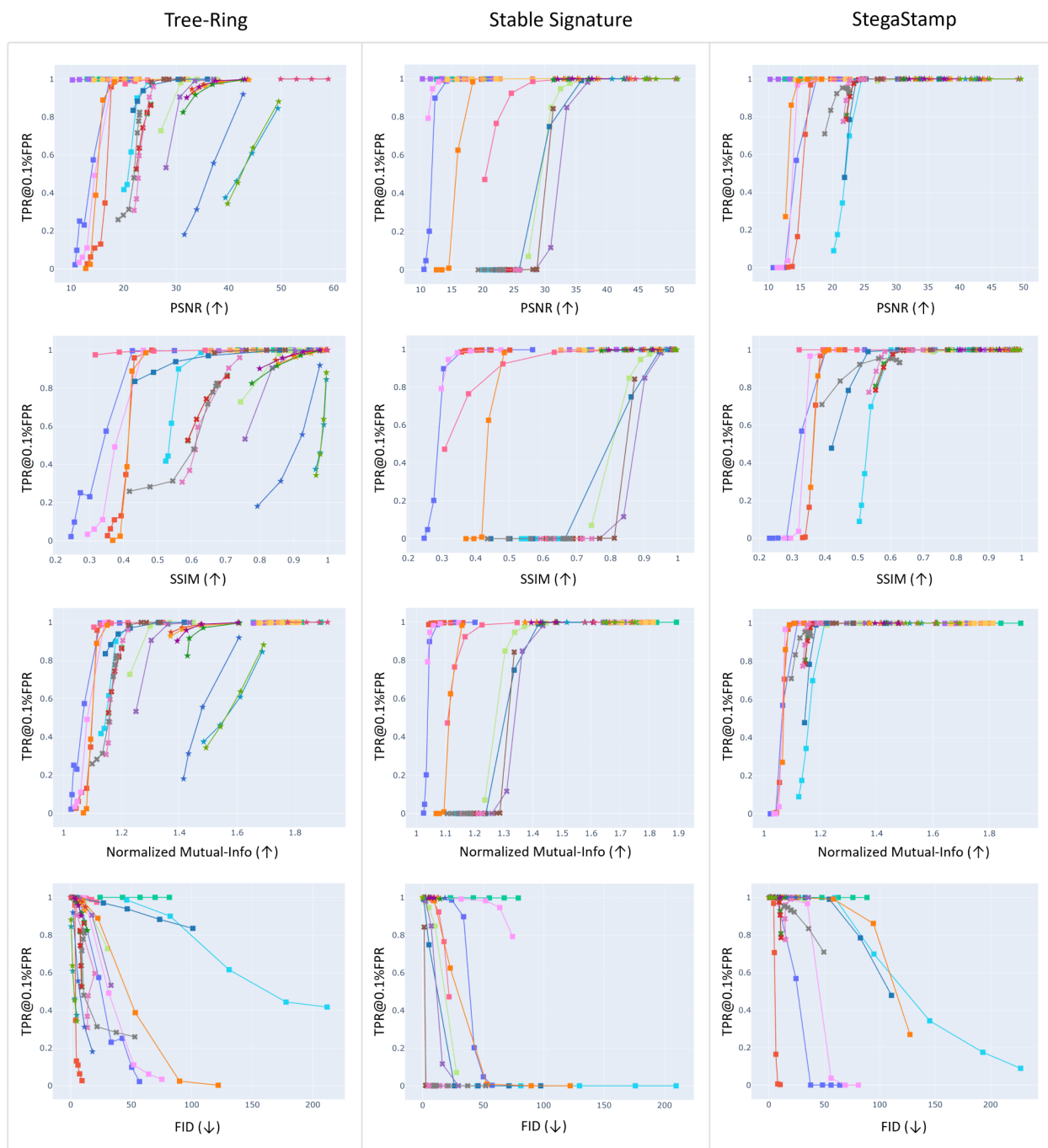


Figure 25. Evaluation on DiffusionDB dataset under the detection setup (part 1).

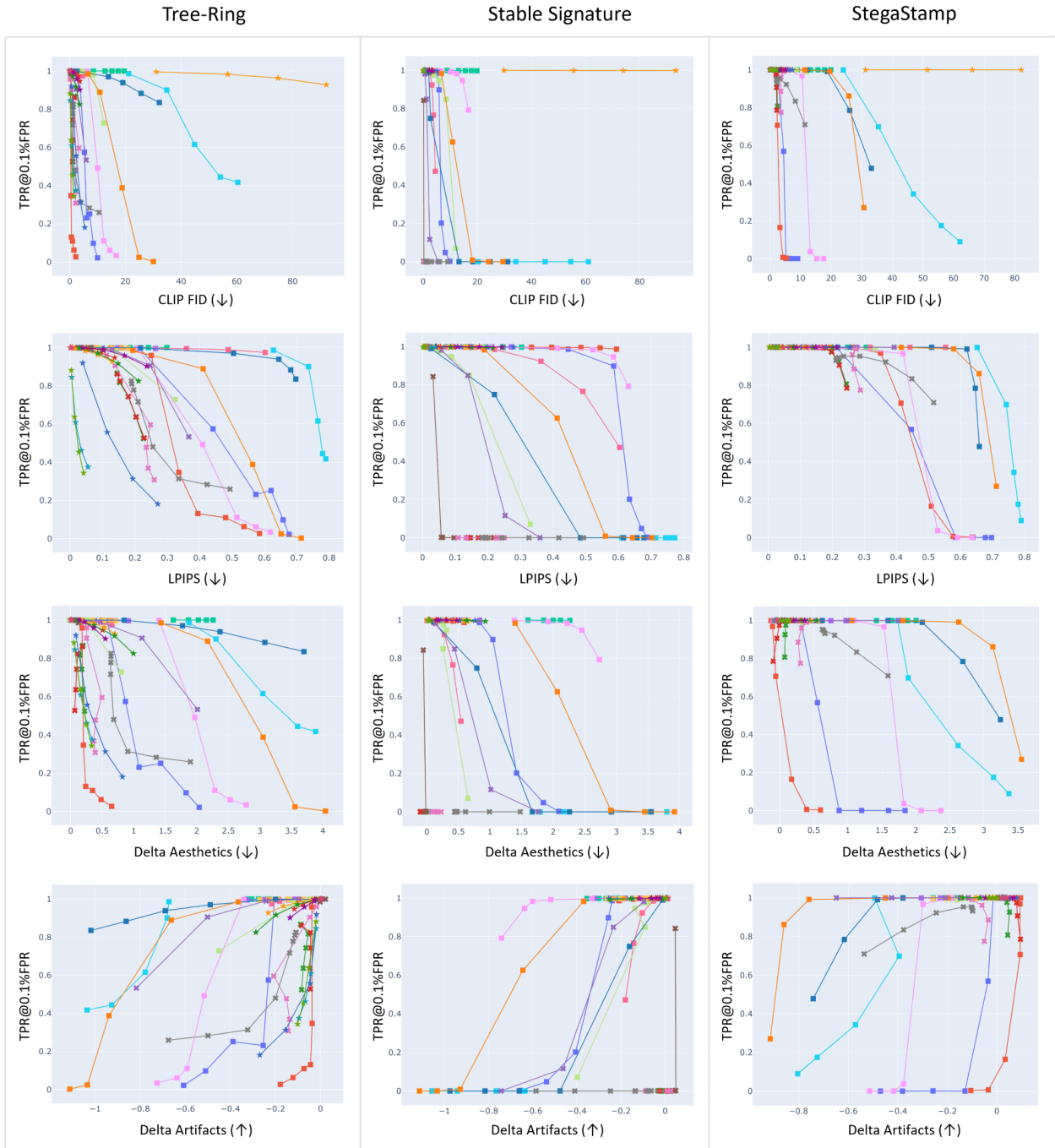
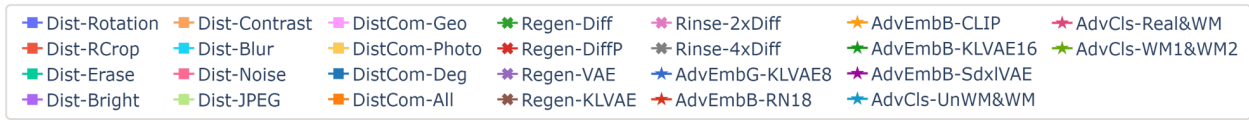


Figure 26. Evaluation on DiffusionDB dataset under the detection setup (part 2).

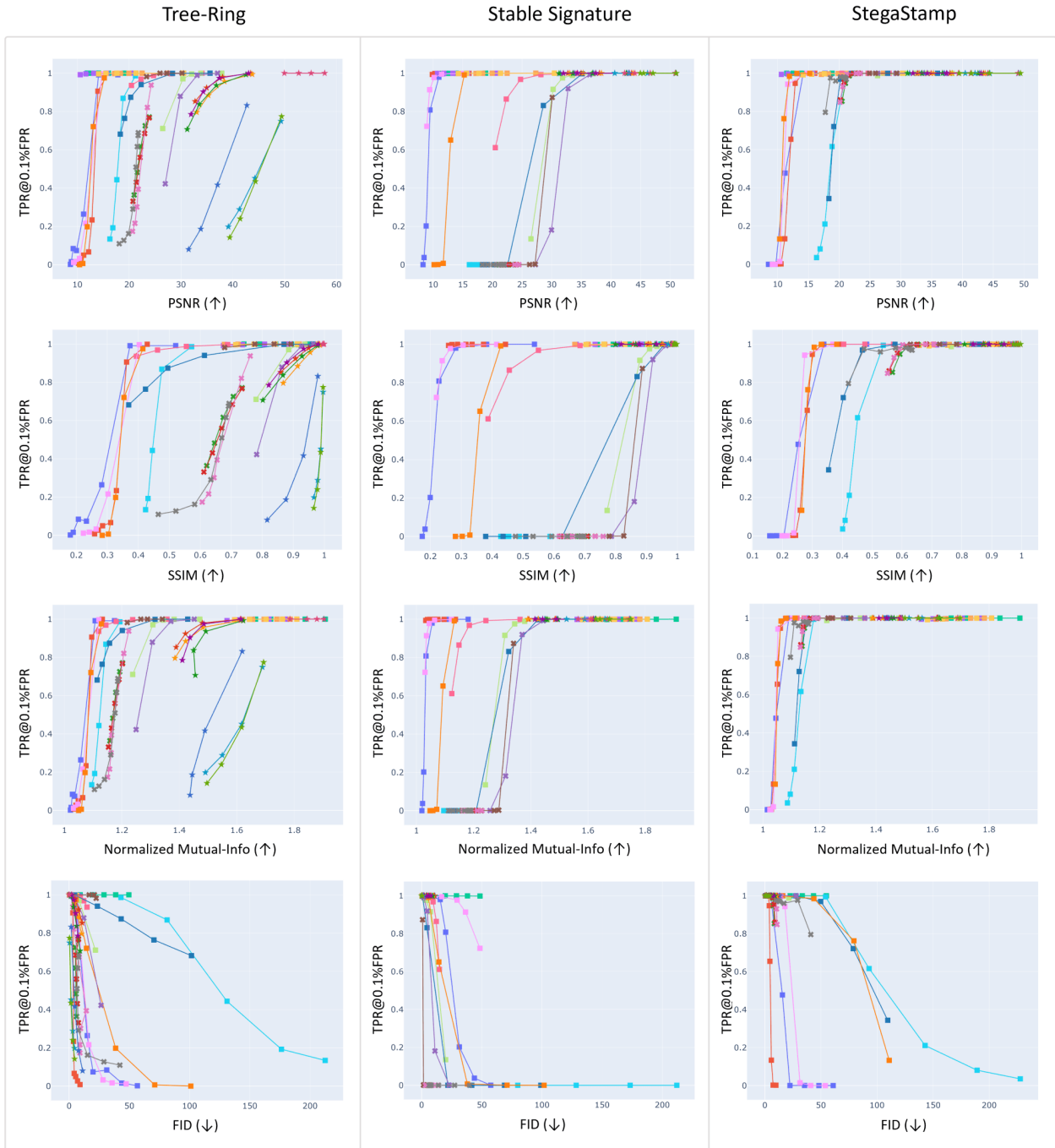
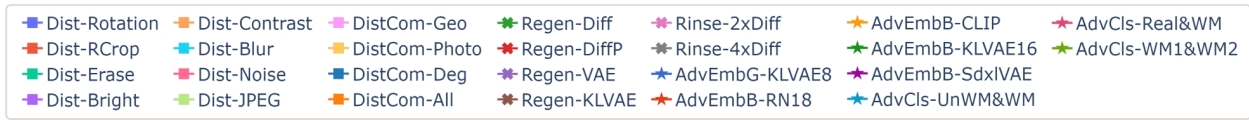


Figure 27. Evaluation on MS-COCO dataset under the detection setup (part 1).

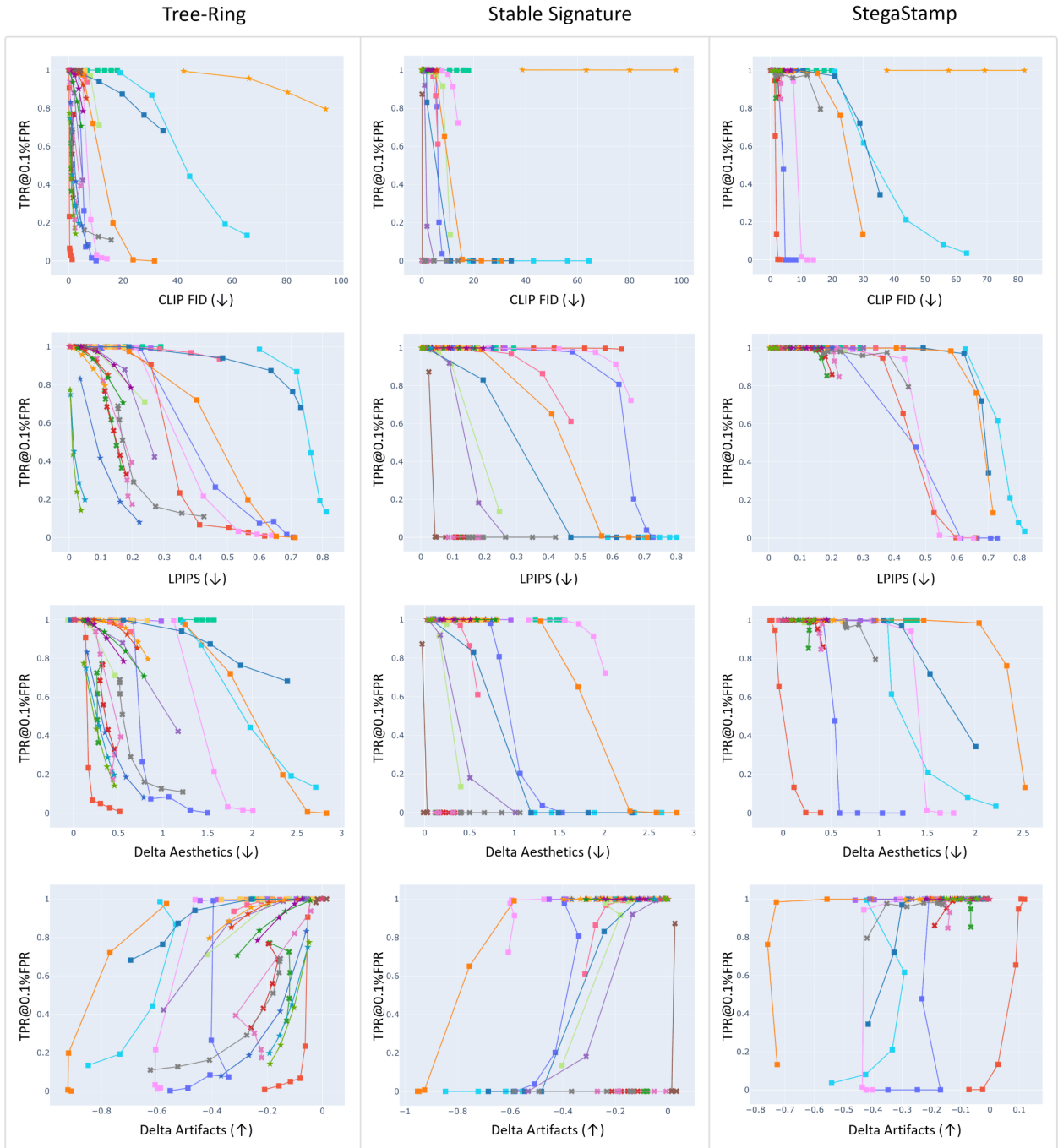
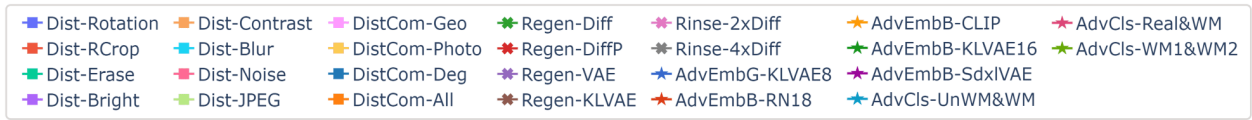


Figure 28. Evaluation on MS-COCO dataset under the detection setup (part 2).

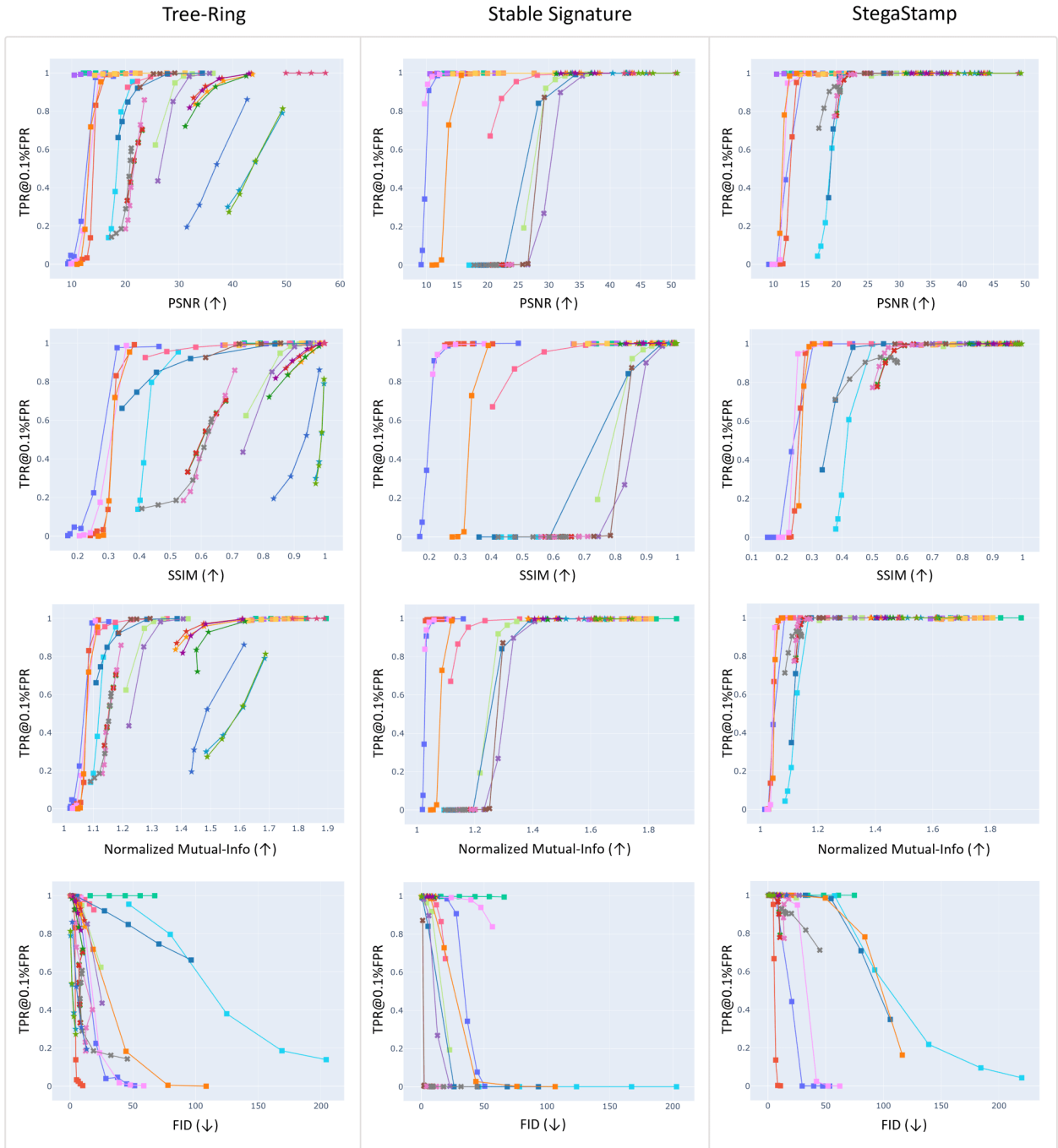
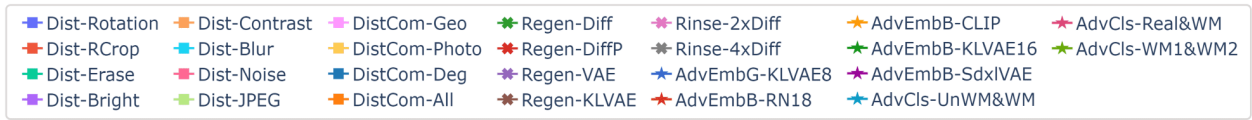


Figure 29. Evaluation on DALL-E3 dataset under the detection setup (part 1).

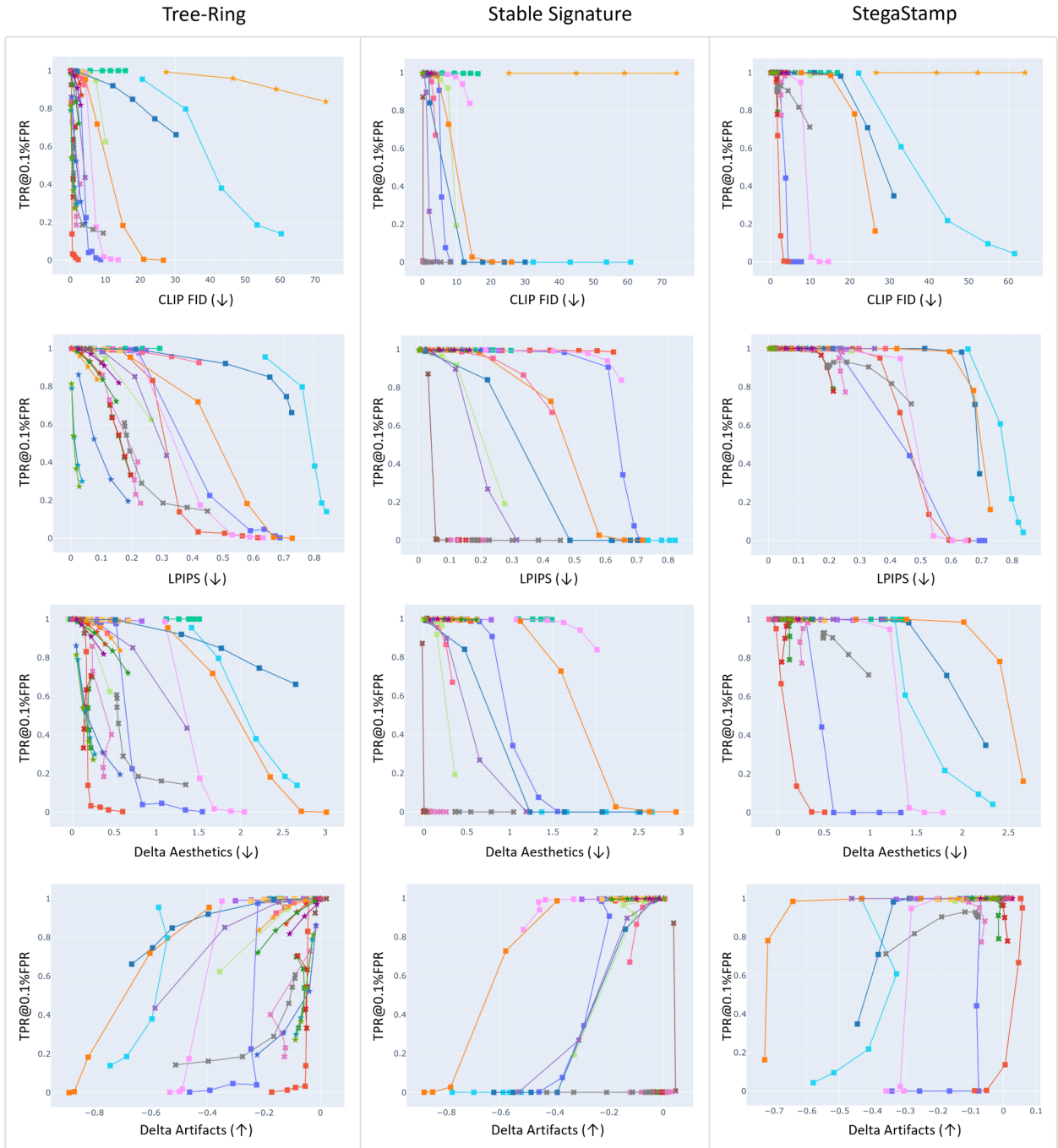
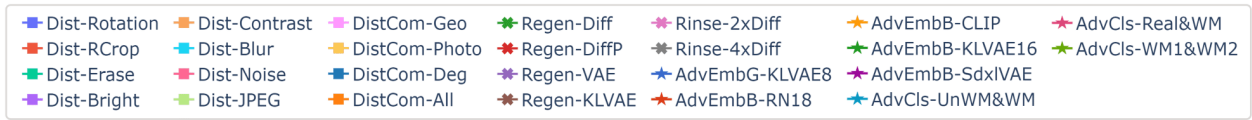


Figure 30. Evaluation on DALL-E3 dataset under the detection setup (part 2).

